

Novel 1,5-diaryl pyrazole-3-carboxamides as selective COX-2/sEH inhibitors with analgesic, anti-inflammatory, and lower cardiotoxicity effects

O.M. Hendawy^{1,2}, Hesham A.M. Gomaa¹, Sami I. Alzarea¹, Mutariah S. Alshammari³, Fatma A.M. Mohamed^{4,5}, Yaser A. Mostafa⁶, Ahmed H. Abdelazeem^{7,8}, Mostafa H. Abdelrahman⁹, Laurent Trembleau^{10*}, Bahaa G. M. Youssif^{6*}

¹Department of Pharmacology, College of Pharmacy, Jouf University, Sakaka, Aljouf 72341, Saudi Arabia; ²Department of Clinical Pharmacology, Faculty of Medicine, Beni-Suef University, Egypt; ³Department of Chemistry, College of Science, Jouf University, Sakaka, Aljouf 72341, Saudi Arabia; ⁴Clinical Laboratory Science Department, College of Applied Medical Sciences, Jouf University; Aljouf 72341 Saudi Arabia; ⁵Chemistry Department, Faculty of Science, Alexandria University, Alexandria-21321, Egypt; ⁶Pharmaceutical Organic Chemistry Department, Faculty of Pharmacy, Assiut University, Assiut 71526, Egypt; ⁷Department of Medicinal Chemistry, Faculty of Pharmacy, Beni-Suef University, Beni-Suef 62514, Egypt; ⁸Department of Pharmaceutical Sciences, College of Pharmacy, Riyadh Elm University, Riyadh 11681, Saudi Arabia; ⁹Department of Pharmaceutical Organic Chemistry, Faculty of Pharmacy, Al-Azhar University, Assiut 71524, Egypt; ¹⁰School of Natural and Computing Sciences, University of Aberdeen, Meston Building, Aberdeen, AB24 3UE, United Kingdom.

**To whom correspondence should be addressed*

Laurent Trembleau, Ph.D. University of Aberdeen, Chemistry Department, The SyMBioSIS Group, Meston Building, Meston Walk, Aberdeen, AB24 3UE, United Kingdom.

Tel.: +44-(0)12242922

E-mail address: l.trembleau@abdn.ac.uk

Bahaa G. M. Youssif, Ph.D. Pharmaceutical Organic Chemistry Department, Faculty of Pharmacy, Assiut University, Assiut 71526, Egypt.

Tel.: (002)-01098294419

E-mail address: bahaa.youssif@pharm.aun.edu.eg, bgyoussif@ju.edu.sa

Abstract

COX-2 selective drugs have been withdrawn from the market due to cardiovascular side effects, just a few years after their discovery. As a result, a new series of 1,5-diaryl pyrazole carboxamides **19-31** was synthesized as selective COX-2/sEH inhibitors with analgesic, anti-inflammatory, and lower cardiotoxic properties. The target compounds were synthesized and tested *in vitro* against COX-1, COX-2, and sEH enzymes. Compounds **20**, **22** and **29** exhibited the most substantial COX-2 inhibitory activity (IC_{50} values: 0.82-1.12 μ M) and had SIs of 13, 18, and 16, respectively, (c.f. celecoxib; SI = 8). Moreover, compounds **20**, **22**, and **29** were the most potent dual COX-2/sEH inhibitors, with IC_{50} values of 0.95, 0.80, and 0.85 nM against sEH, respectively, and were more potent than the standard AUDA (IC_{50} = 1.2 nM). Furthermore, *in vivo* studies revealed that these compounds were the most active as analgesic/anti-inflammatory derivatives with a good cardioprotective profile against cardiac biomarkers and inflammatory cytokines. Finally, the most active dual inhibitors were docked inside COX-2/sEH active sites to explain their binding modes.

Keywords: Pyrazoles, NSAIDS, Cardiomyopathy, COX-2/sEH.

1- Introduction

The market for new peripheral analgesics and anti-inflammatory agents is still a challenge, as they are used not only to manage inflammation and pain, but also to help with the symptomatic treatment of a variety of disorders, such as cancer, gout, cardiovascular disease, and so on. As a result, pharmaceutical research will increasingly focus on compounds that can treat both acute and chronic pain [1-3]. The clinical application of non-selective NSAID is restricted especially for patients with a history of peptic ulcer, as they are accompanied by primary and secondary unwanted side effects. They act by depriving the cyclooxygenase enzyme isoforms COX-1 and COX-2, which prevent the production of cytoprotective prostaglandins (PGs). As a result, the development of selective COX-2 inhibitors was regarded as a promising approach for avoiding the adverse effects of NSAIDs on the gastrointestinal system [4,5]. However, due to a decrease in the production of the protective prostacyclin (PGI₂), there is an increased incidence of cardiovascular side effects [6,7]. Soluble epoxide hydrolase (sEH) is a pervasive enzyme found throughout the body, with the highest concentrations found in the liver, renal, lungs, and vascular tissues [8]. This enzyme is specific for aliphatic epoxides of fatty acids, such as epoxyeicosatrienoic acids (EETs), which are a metabolic derivative of Arachidonic Acid (AA) [9, 10]. EETs have been shown to have analgesic and anti-inflammatory properties as well as cardiovascular protective effects [11]. Furthermore, EETs demonstrated pro-angiogenic properties, which are linked to a cardioprotective effect in chronic phases [12]. The enzyme sEH mediates the addition of water to EETs, resulting in dihydroxyeicosatrienoic acids (DHETs) with reduced biological activity [13]. As a result, inhibiting the enzyme sEH causes an increase in EET concentration, which has anti-inflammatory, pain-relieving, and cardiovascular risk-lowering properties [14].

Pyrazole framework plays an essential role in biologically active compounds and therefore represents an interesting template for medicinal chemistry. Many pyrazole derivatives are known to exhibit a wide range of biological properties such as anti-inflammatory [15-18], analgesic [19], and anticancer [20, 21]. The pyrazole ring is present as the core in a variety of leading drugs such as selective COX-2 inhibitor (Celecoxib) [22, 23], non-steroidal anti-inflammatory drug (Lonazolac) [24], phosphodiesterase inhibitor (Sildenafil) [25], and antiobesity drug (Rimonabant) [26, 27].

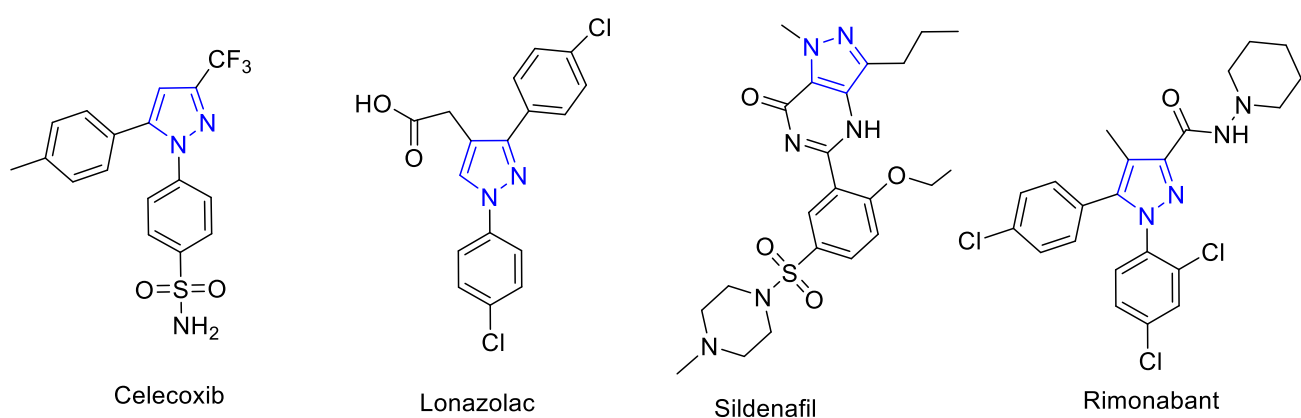


Fig. 1. Structures of pharmaceutically active compounds containing pyrazole moiety

Encouraged by these findings, and as part of our ongoing research program [12, 28-30] to find new and improved anti-inflammatory agents, we present here the synthesis and pharmacological evaluation of novel 1,5-diaryl pyrazole-3-carboxamide derivatives (**19-31**, **Fig. 2**) as safer and potent analgesic and anti-inflammatory agents. The newly synthesized derivatives were tested *in vitro* for their inhibitory effects on COX-1, COX-2, and sEH. Compounds with strong inhibitory activity were chosen for testing for analgesic, anti-inflammatory, ulcerogenicity, inhibition of inflammatory cytokines, and cardiovascular effects *in vivo*. Finally, a molecular docking study was presented in order to provide a plausible explanation for the differences in bioactivity between our newly synthesized derivatives against both COX-2 and sEH enzymes.

1.1. Rational Design

Recently, the design of a single modulator agent pointing different targets using multi-target directed ligand (MTDL) technique constitutes one of the most prominent techniques in recent medicinal chemistry research. Firstly, identification of each target pharmacophore is the critical step in the MTDL technique, followed by hybridization of the pharmacophoric moieties which is carried out to provide one molecule able to simultaneously hit the different targets. Herein, our dual COX-2/sEH inhibitor design depends on the determination of COX-2/sEH pharmacophores through selective COX-2 [31], selective sEH and recently reported dual COX-2/sEH inhibitors [12]. Consequently, COX-2 pharmacophoric moiety is represented as diaryl-heterocycle, which accomplishes the required Y-shaped structure. Additionally, its adhesion to the five-membered pyrazole nucleus which is known for its precarious role in COX-2 activity. On the other hand, sEH pharmacophoric moiety was detected through the inspection study of known selective sEH inhibitors' interaction inside 3D protein structure and the reported dual COX-2/sEH inhibitors. Noticeably, these studies exposed that amide moiety is an essential chemical unit in enzyme interaction. Moreover, its adhesion to aromatic residue through a short linker is a noticeable point needed to be examined. So, we hybridize both COX-2/sEH pharmacophoric moieties together along with study the effect of linker elongation between amide and aromatic residue on both COX-2/sEH activities as shown in **Fig. 2**.

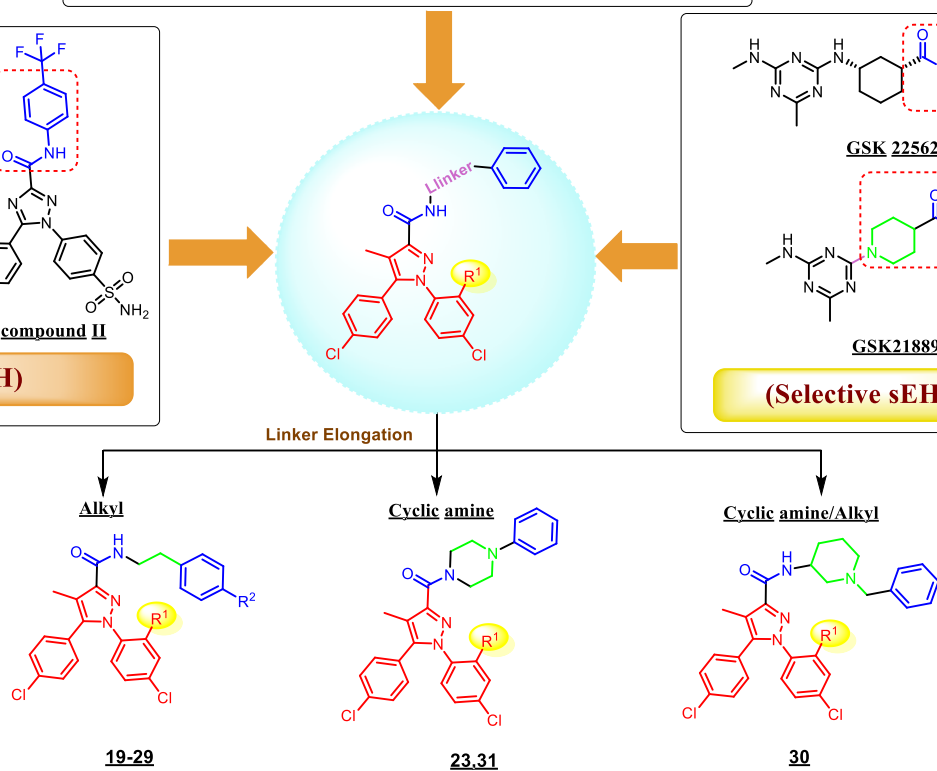
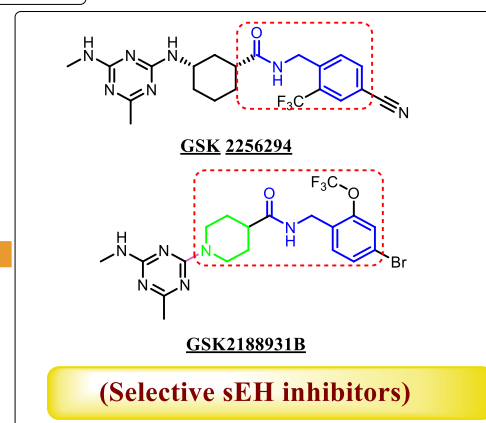
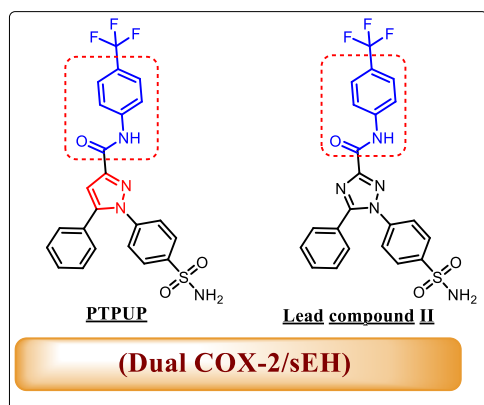
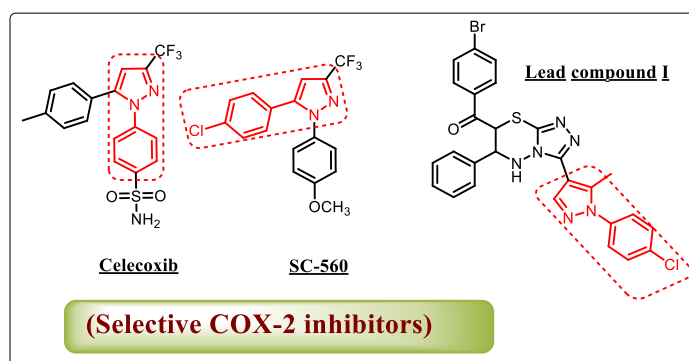


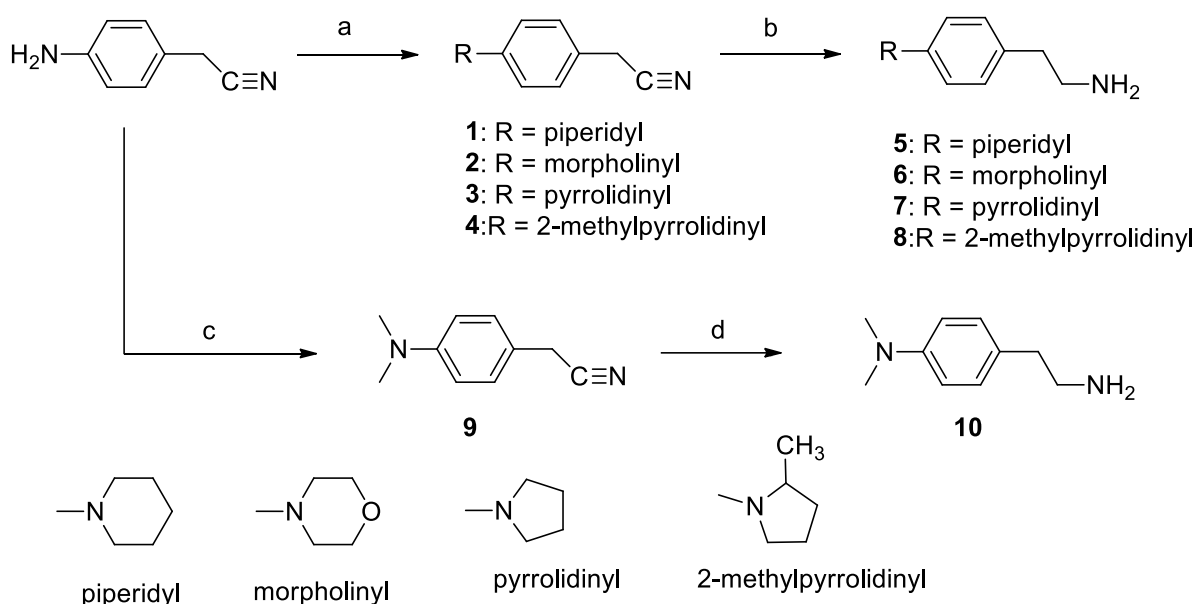
Fig. 2. Rational design of compounds 19-31

2. Results and discussion

2.1. Chemistry

In this study, pyrazole-3-carboxamides were prepared using substituted pyrazole-3-carboxylic acids by coupling to a series of amines. All the compounds were satisfactorily characterized by nuclear magnetic resonance (NMR) spectroscopy and high-resolution mass spectrometry (HRMS).

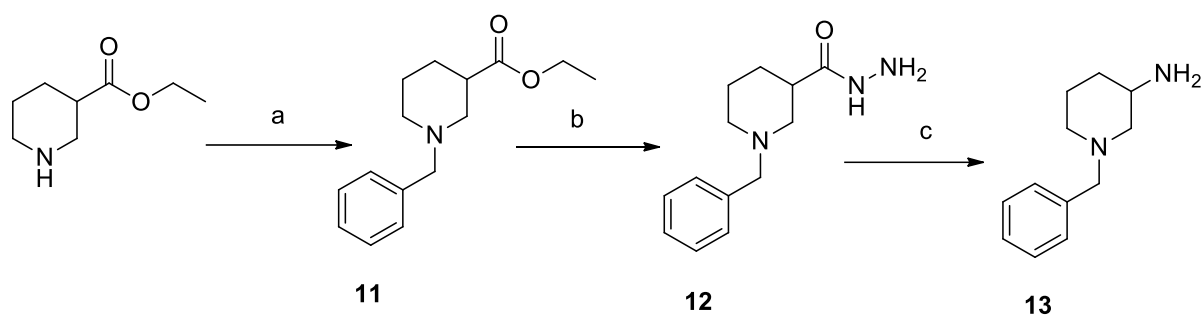
As previously stated, phenethylamine derivatives **5-8** and **10** were synthesized using the general process specified in **Scheme 1** [32].



Scheme 1: Synthesis of phenethylamine derivatives **5-8** and **10**.

Reagents and conditions: (a) 1,5-dibromopentane, bromoethyl ether, 1,4-dibromobutane or 1,4-dibromopentane DIPEA, toluene, reflux, 20 h. (b) LiAlH_4 , Et_2O , 0 °C to room temperature (rt), overnight (c) 37% aqueous formaldehyde, NaBH_3CN , acetic acid, CH_3CN , rt, 3h. (d) LiAlH_4 , Et_2O , 0 °C to rt, overnight.

The preparation of 1-benzyl-3-aminopiperidine was also accomplished using a three-step procedure [33]. ^1H NMR and ^{13}C NMR spectroscopic analyses, as well as high-resolution mass spectrometry, were used to confirm the structures of compounds **11-13**.

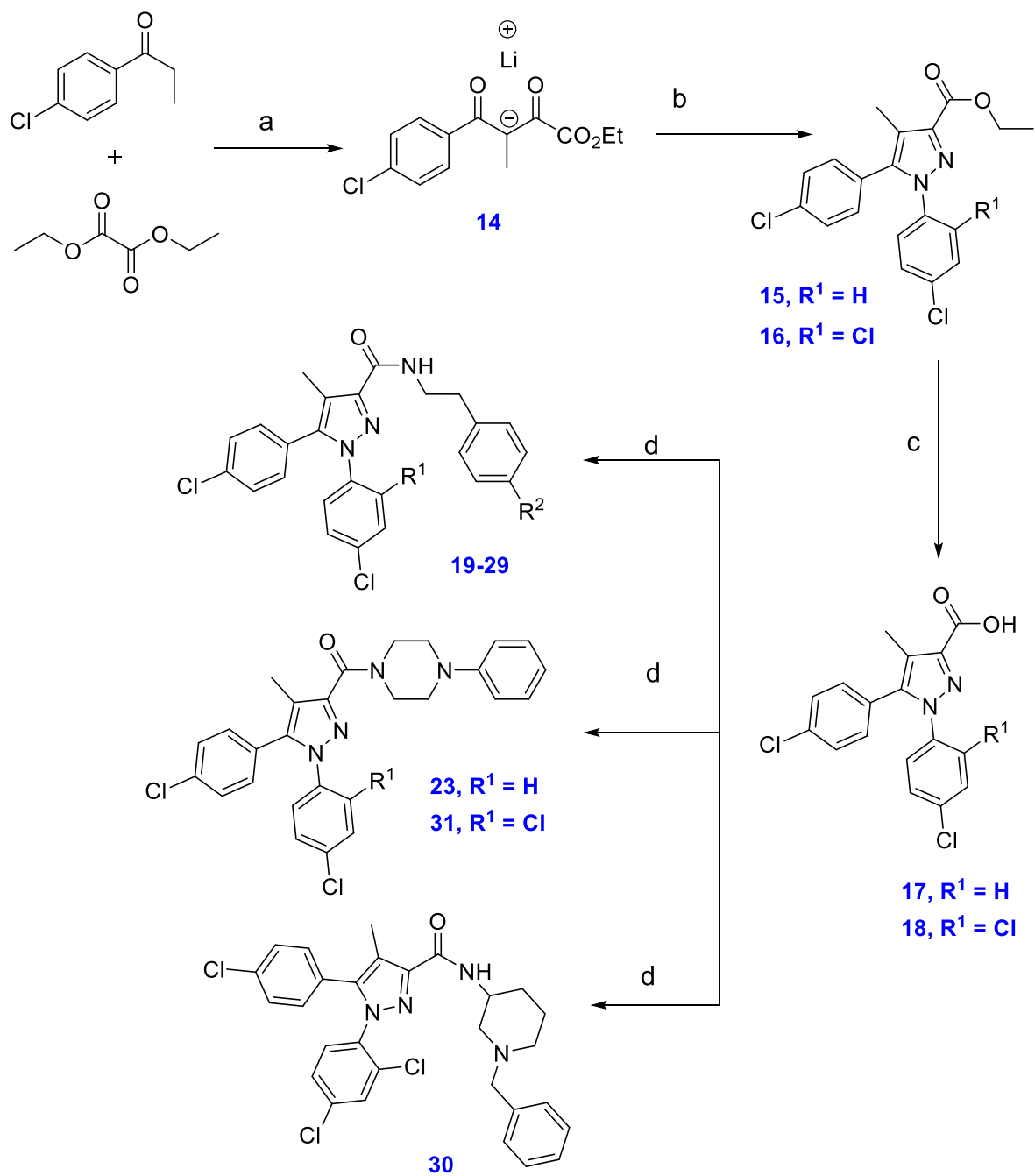


Scheme 2: Synthesis of 1-benzyl-3-aminopiperidine **13**

Reagents and conditions: a) Benzyl bromide, Na_2CO_3 , DCM / H_2O (2:1), reflux, 3 h. (b) NH_2NH_2 , ethanol, reflux, 3 h. (c) NaNO_2 , TFA, H_2O , 0 °C for 2 h then 80 °C for 2 h.

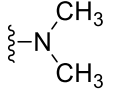
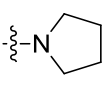
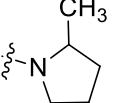
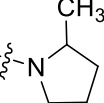
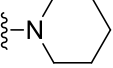
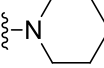
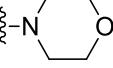
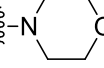
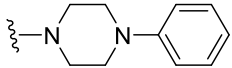
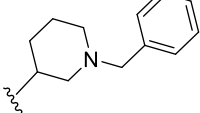
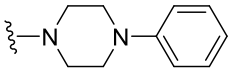
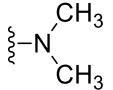
The synthesis of pyrazole-3-carboxamide derivatives **19-31** is depicted in **Scheme 3**. The pyrazole-3-carboxylic acid esters **15** and **16** were prepared by treating *p*-chloropropiophenone with diethyl oxalate in the presence of lithium bis(trimethylsilyl)amide (LHMDS) as a base, yielding lithium salt **14** which was then coupled in ethanol with 2,4-dichlorophenyl hydrazine HCl or 4-chlorophenylhydrazine HCl, followed by intramolecular cyclization in acetic acid under refluxing conditions to yield the pyrazole esters **15** and **16**. The ^1H NMR spectrum of **15** as an example of these esters showed singlet equivalent to three protons at δ 2.31 ppm which assigned to methyl group and ethoxy group with a quartet at 4.42 ppm and a triplet at 1.39 ppm as well as aromatic protons. The structure of **15** was also confirmed by HRESI-MS which gave a molecular ion m/z 409.0277 $[\text{M}+\text{H}]^+$ which is consistent with the molecular formula $\text{C}_{19}\text{H}_{16}\text{Cl}_3\text{N}_2\text{O}_2$. Under standard conditions, basic hydrolysis was used to convert these esters to the corresponding carboxylic acids **17** and **18**. Analysis of the ^1H NMR spectrum of **17** as an example of ester hydrolysis revealed the disappearance of ethoxy protons in its ester starting material. Furthermore, the ethoxy carbon signals were also disappeared in the ^{13}C NMR spectrum of the product, indicating successful deprotection of the carboxylic acid group. The coupling reaction between pyrazole-3-carboxylic acids **17** and **18** and appropriate amines was performed by using (benzotriazol-1-yloxy)tris

(dimethylamino)phosphonium hexafluorophosphate (BOP) as the coupling reagent in the presence of DIPEA to give the targeted pyrazole-3-carboxamides **19-31** in very good yields. All the structures of pyrazole-3-carboxamides were confirmed by NMR spectroscopic and high-resolution mass spectrometry. Compound **28** as an example of this series was identified by the appearance of extra peaks which were not presented in the carboxylic acid starting material **18** in both the ^1H NMR and ^{13}C NMR spectra as well as via HRESI mass spectrometry. The ^1H NMR spectrum of **28** revealed the appearance of two sets of doublets at 7.12 and 6.88 ppm with coupling constant of $J = 8.6$ Hz each assigned to the phenyl protons which is indicative of aromatic *para*-disubstitution, two signals of two protons integration each at 3.63 (q) and 2.83 (t) ppm attributed to NHCH_2CH_2 group, and piperidinyl protons. The structure of **28** was also confirmed by HRESI-MS which gave a molecular ion m/z 567.1479 $[\text{M}+\text{H}]^+$ consistent with the molecular formula $\text{C}_{30}\text{H}_{30}\text{Cl}_3\text{N}_4\text{O}$ of the desired product.



Scheme 3: Synthesis of pyrazole-3-carboxamides 19-31

Reagents and conditions: (a) LHMDS $-78\text{ }^{\circ}\text{C}$ to rt, 16 h. (b) 2,4-dichlorophenyl hydrazine HCl or 4-dichlorophenylhydrazine HCl, EtOH, rt, 20 h, then AcOH, reflux, 24 h. (c) KOH, MeOH, $60\text{ }^{\circ}\text{C}$, 4 h. (d) Appropriate amine, BOP, DIPEA, DCM, overnight, rt.

Compound No.	R ¹	R ²	Compound No.	R ¹	R ²
19	H		26	Cl	
20	H		27	Cl	
21	H		28	Cl	
22	H		29	Cl	
23	H		30	Cl	
24	Cl	H	31	Cl	
25	Cl				

4.2. Pharmacological Evaluations

2.2.1. *In vitro* assays

2.2.1.1. COX-1 and COX-2 inhibition assays

All the newly synthesized 1,5-diaryl pyrazole-3-carboxamides **19-31** were screened for *in vitro* COX-1/COX-2 inhibition assays, using the COX-1/COX-2 (human) Inhibitor Screening Assay Kit [34]. The half-maximal inhibitor concentrations IC_{50} values were computed as the means of three determinations acquired, and the selectivity index (SI) values were calculated as IC_{50} (COX-1)/ IC_{50} (COX-2), **Table 1**. The IC_{50} values of the screened compounds were obtained and compared to the reference drug celecoxib.

The *in vitro* assay revealed that many of the synthesized compounds exhibited significant efficacy and selectivity against the COX-2 isoform. Compounds **20-22**, **24**, and **29** are extremely strong COX-2 inhibitors with IC_{50} values in the sub-micromolar range. Furthermore, they demonstrated clear preferential COX-2 over COX-1 inhibition with SIs of 13, 9, 18, 6, and 16, respectively. Compounds **20**, **21**, **22**, and **29** were particularly interesting because they exhibited the most substantial COX-2 inhibitory activity (IC_{50} values: 0.82-1.12 μ M). They had SIs of 13, 9, 18, and 16, respectively, which were 1.15-2.25-fold greater than celecoxib (SI = 8, **Table 1**). The structural activity relationship analysis of the new 1,5-diaryl pyrazole-3-carboxamides **19-31** revealed that the substitution pattern on the phenyl group of the phenethyl moiety was a crucial element for the COX-2 inhibition and selectivity. The 4-morpholin-4-yl phenethyl derivatives **22** ($R^1 = H$) and **29** ($R^1 = Cl$) were the most potent among the synthesized derivatives, with IC_{50} values of 0.74 and 0.82 μ M against the COX-2 isoform and SI of **19** and **16**, respectively, and were more potent than the reference celecoxib ($IC_{50} = 0.88$, SI = 8). The unsubstituted derivative **24** was roughly twice less potent than **22** and **29**, with an IC_{50} of 1.57 μ M against the COX-2 isoform and a SI of 6, whereas the 4-

dimethylamino derivatives **19** ($R^1 = H$) and **25** ($R^1 = Cl$) had IC_{50} values of 2.47 and 1.68, respectively, and SI of 3 and 5, respectively. The presence of 2-methylpyrrolidine or piperidine groups on the phenethyl moiety of 1,5-bis(4-chlorophenyl)-pyrazole-3-carboxamides **20** and **21** significantly increased COX-2 selectivity over the reference drug celecoxib.

The COX-2 selectivity was reduced by at least 4-folds when the 4-morpholin-4-yl moiety in compound **29** was replaced by 4-pyrrolidin-1-yl or 4-piperidin-1-yl in compounds **26** and **28**, respectively. Furthermore, among the studied compounds, the 4-phenylpiperazine carbonyl derivatives **23** and **31**, as well as the benzylpiperidine-3-yl carbonyl derivative **30**, had the highest IC_{50} values (lowest inhibitory effect), implying that the *N*-phenethyl carboxamide architecture is important for COX-2 inhibition and selectivity.

2.2.1.2. Soluble epoxide hydrolase (sEH) assay

The inhibitory activity of the synthesized derivatives **19-31** against sEH enzyme using a cell-based assay kit [35] was evaluated *in vitro* and presented as IC_{50} values in **Table 1**. In comparison to the reference AUDA ($IC_{50} = 1.2$ nM), most of the compounds examined demonstrated good inhibitory activity against sEH, with IC_{50} values ranging from 0.80 to 4.70 nM. The *in vitro* sEH assay results complemented the COX-2 inhibitory activity assay, which revealed that compounds **20-22**, **24**, and **29** with the highest COX-2 inhibition and selectivity were the most potent sEH inhibitors with IC_{50} values ranging from 0.80 to 1.2 nM. Compounds **20**, **22**, and **29** were the most potent dual COX-2/sEH inhibitors, with IC_{50} values of 0.95, 0.80, and 0.85 nM against sEH, respectively, and were more potent than the standard AUDA ($IC_{50} = 1.2$ nM). According to the results, the presence of *N*-phenethyl carboxamide architecture is required for sEH inhibition. As a result, compounds **23** and **31** containing 4-phenylpiperazine carbonyl in the 3-position of diaryl pyrazole, as well as the benzylpiperidine-3-yl carbonyl derivative **30**, had the lowest inhibitory effects.

Table 1: COX-1/COX-2 and sEH inhibitory activities of **19-31**, Celecoxib, and AUDA.

Compound No.	COX-1 (IC₅₀, μM)	COX-2 (IC₅₀, μM)	SI^a	sEH^b (IC₅₀, nM)
19	8.22	2.47	3.32	1.57±0.02
20	11.98	0.89	13.46	0.95±0.01
21	10.53	1.12	9.40	1.10±0.01
22	13.65	0.74	18.44	0.80±0.01
23	8.33	2.65	3.14	3.20±0.02
24	9.28	1.57	5.91	1.20±0.60
25	8.89	1.68	5.29	1.35±0.01
26	8.20	1.98	4.14	1.50±0.01
27	7.93	2.17	3.65	1.60±0.02
28	8.17	1.83	4.46	1.80±0.01
29	12.75	0.82	15.55	0.85±0.01
30	7.95	2.33	3.41	4.10±0.02
31	7.98	3.23	2.47	4.70±0.02
Celecoxib	7.32	0.88	8.31	260±14.60
AUDA	--	--		1.2

^aSelectivity index was calculated by dividing COX-1 IC₅₀ by COX-2 IC₅₀.

^b the values are the mean ± SEM (n = 3).

2.2.2. *In vivo* assays

2.2.2.1. Analgesic activity

Based on the results of previous *in vitro* tests, five compounds (**20-22**, **24**, and **29**) were selected to be examined for *in vivo* analgesic activity using the acetic acid-induced writhing method [36]. The reduction in acetic acid-induced writhing episodes was used to determine the efficacy and potency of the tested compounds. **Table 2** summarizes the obtained results. When compared to the reference drug, celecoxib, which had 13.43% inhibition in the number of writhing, the results revealed that all of the compounds tested had good analgesic activity, with percent inhibition in the number of writhing ranging from 34% to 71%. Compounds **20**,

22, and **29**, the most potent dual COX-2/sEH inhibitors *in vitro*, also triggered the highest analgesic activity with % inhibition of 62.68, 71.64, 67.16, respectively, and potencies of 4.66, 5.33, and 5, respectively.

Table 2: Analgesic activity of compounds **19-31**

Compound Code	No. of writhes ^a (mean ± SE)	% Inhibition	Potency ^b
20	12.50±0.60	62.68	4.66
21	19.50±0.50	41.79	3.11
22	9.50±0.40	71.64	5.33
24	22.00±0.60	34.32	2.55
29	11.00±0.40	67.16	5.00
Celecoxib	29.00±0.60	13.43	1
Control	33.50±0.80	--	--

^a Values are given as mean ± SE.

^b Potency are calculated according to equation of relative potency % = % of inhibition of tested compound / % of inhibition of reference x 100

2.2.2.2. Anti-inflammatory assay

Five compounds (**20-22**, **24**, and **29**) were selected to be examined for *in vivo* anti-inflammatory activity using Winter et al. carrageen-induced paw edema bioassay method [37]. The compounds' efficacy was measured as the decrease in edema paw volume and calculated as edema inhibition percentage (EI %) after 1, 3, and 5 h of carrageenan injection versus the standard drug celecoxib. Results demonstrated that the five tested compounds showed potent anti-inflammatory activities with EI% in the range of 38% to 71%. After 5 h of compound administration, the anti-inflammatory activities of compounds **20**, **22**, and **29** outperformed celecoxib. They showed a rapid onset of action and a long-lasting effect until the fifth hour after the compounds were given. Compound **22** was equipotent to celecoxib

after the first hour of administration, but it had more potent anti-inflammatory activity than celecoxib after the third and fifth hours, (**Table 3**). Based on our findings, the 1,5-diaryl pyrazole scaffold with *N*-phenethyl carboxamide architecture is a promising lead for developing highly efficient COX-2/sEH inhibitors as potent anti-inflammatory agents.

Table 3: The percentages of edema inhibition of compounds **20-22**, **24**, and **29**

Compound No.	Baseline	% of Edema inhibition		
	Paw diameter (mm) ± SE	1h	3h	5h
Control	2.76±0.09	--	--	--
20	2.30±0.06	24	49	62
21	2.83±0.09	19	37	43
22	2.01±0.09	32	59	71
24	2.98±0.09	17	32	38
29	2.08±0.07	29	52	65
Celecoxib	2.09±0.07	40	54	22

The anti-inflammatory activity (the percentage of edema inhibition) was calculated according to the following equation:

$$\% \text{ Edema} = [(V_R - V_L) \text{ control} - (V_R - V_L) \text{ treated}] / (V_R - V_L) \text{ control} \times 100$$

Where, V_R : Average right paw thickness, V_L : Average left paw thickness.

2.3. Gastric ulcerogenic activity

The two most common side effects of chronic administration of NSAIDs are gastrointestinal erosion and ulcers. As a result, we were curious about the ulcerogenic potential of the most potent compounds, **20**, **22**, and **29**, when administered orally. The ulcerogenic effects of these compounds were assessed by macroscopic observation of rat's intestinal mucosa following the oral use of 10 mg/kg of **20**, **22**, and **29** as well as indomethacin and celecoxib [38, 39].

Compounds **22** and **29** showed no ulceration from the isolated rat stomach, whereas compound **20** showed moderate hyperemia without gross ulceration (**Table 4**). Compounds **20**, **22**, and **29** were discovered to have a potent and dual COX-2/sEH inhibitory profile, as well as potent anti-inflammatory activity with no gastric toxicity.

Table 4. Ulcerogenic effects of compounds **20**, **22** and **29**.

Groups	Score	
	No. of gastric ulcers	Severity lesions
Control	0	0
20	0.4±0.01	0.6±0.01
22	0	0
29	0	0
Celecoxib	2.5±0.10	5.8±0.20
Indomethacin	8.5±0.40	12.5±0.70

2.4. Effect on inflammatory cytokines

2.4.1. Prostaglandin E_2 (PGE_2)

PGE_2 inhibition has been identified as one of the most effective methods of inflammation therapy since high levels of the inflammatory mediator PGE_2 occurs in inflammatory disorders [40, 41]. In addition, recent reports on the significance of reducing PGE_2 in anti-inflammatory effects [42]. A study was conducted on the **20**, **22**, and **29** capacities to inhibit PGE_2 in the PGE_2 serum rat levels in blood samples collected following **5h** of subcutaneous carrageenan injections. **Table 5** estimates and shows the percentage of PGE_2 inhibition. The results obtained showed that compounds **20**, **22**, and **29** had a significant reduction in serum PGE_2 (% inhibition = 73-78), which was greater than the reference celecoxib (72%).

2.4.2. Determination of rat serum TNF- α and IL-6

Typical pro-inflammatory cytokines (TNF- α and IL-6) have been found to identify the occurrence of inflammation and their role in chronic diseases [43]. The overall anti-inflammatory impact is dependent in part on lowering the levels of these inflammatory indicators in the plasma [44]. The serum concentrations of TNF- α and IL-6 in blood samples collected from rats treated with chemicals **20**, **22**, and **29** were evaluated in the current investigation (**Table 5**). Compounds **20**, **22**, and **29** significantly reduced rat serum concentrations of both TNF- α (% inhibition = 72-75) and IL-6 (% inhibition = 78-80) which were more active than celecoxib of 64 and 71, respectively. Compound **22** was the most active compound, with a TNF- α inhibition rate of 77 compared to celecoxib (% TNF- α inhibition = 64) and decreasing serum IL-6 concentration at a rate of 80% compared to celecoxib of 71%.

Table 5: PEG₂, TNF- α and IL-6 rat serum concentrations for compounds **20**, **22**, **29** and Celecoxib.

Compound No.	Inflammatory markers [serum concentration (pg/ml), %inhibition]					
	PEG2		TNF α		IL-6	
20	81.52 \pm 2.40 ^b	73	65.70 \pm 2.50 ^{ab}	72	83.79 \pm 4.05 ^{ab}	78
22	65.78 \pm 2.15 ^{abc}	78	53.20 \pm 2.05 ^b	77	76.43 \pm 2.55 ^b	80
29	78.13 \pm 2.40 ^b	74	58.56 \pm 2.93 ^{bc}	75	79.22 \pm 2.05 ^{bc}	79
Celecoxib	84.63 \pm 2.50 ^b	72	83.72 \pm 6.50 ^{ab}	64	110.38 \pm 2.50 ^{ab}	71
Control (pre)	70.98 \pm 1.15	ND	44.62 \pm 1.29	ND	74.10 \pm 2.71	ND
Control (post)	302.15 \pm 10.89 ^a	ND	234.60 \pm 4.16 ^a	ND	376.07 \pm 13.7 ^a	ND

Data are expressed as (mean \pm SE). Statistics were done by One-way ANOVA and confirmed by Turkey's test. PGE; Prostaglandin E, IL-6; Interleukin 6, TNF- α ; Tumor necrosis factor α .

^a $P < 0.05$: Statistically significant from control (pre) group

^b $P < 0.05$: Statistically significant from control (post) group (Carrageenan)

^c $P < 0.05$: Statistically significant from standard group (Celecoxib)

2.5. Cardiovascular evaluation

The celecoxib-induced cardiotoxicity in rats [45, 46] was used to assess the potential cardiovascular risks of the most active compounds **22** and **29**. The heart's response to the tested compounds was expressed as the change in the serum levels of lactate dehydrogenase (LDH), troponine-I (Tn-I), tumor necrosis factor- α (TNF- α), and creatine kinase-MB (CK-MB) at a dose of 100 mg/kg of tested compounds as well as celecoxib. **Table 6** displays the obtained results.

Celecoxib treatment resulted in a significant increase in the diagnostic biomarkers of cardiomyopathy (Tn-I, LDH, and CK-MB) when compared to normal control [47-49]. Compounds **22** and **29**, on the other hand, caused no significant changes in the levels of two of these biomarkers (LDH and CK-MB) when compared to the control, indicating their lower

cardiotoxic side effects. Furthermore, compounds **22** and **29** significantly reduced the serum concentration of TNF- α , a key player in the inflammatory response and cardiac depression [50], with % inhibition of 77% and 75%, respectively, when compared to celecoxib (% inhibition = 64%), as shown in **Table 5**. Based on these findings, the proposed scaffold could be a promising starting point for the development of selective COX-2/sEH inhibitors as potent analgesic/anti-inflammatory agents with lower cardiotoxicity.

Table 6: Measurements of serum Tn-I, LDH and CK-MB in **22**, **29** and celecoxib.

Group	Troponine-I (pg/ml)	LDH (IU/L)	CK-MB (IU/L)
Normal control	75±05	1536±100	16±2.50
Celecoxib	340±12 ^a	2100±100 ^a	96±04 ^a
22	105±08 ^b	1375±30 ^b	15±2.5 ^b
29	130±04 ^b	1500±25 ^b	20±04 ^b

Data analyzed by one-way ANOVA test (n = 6).

^a Significantly different from normal control group at p < 0.05.

^b Significantly different from celecoxib group at p < 0.05.

2.6. Molecular docking study

To provide a plausible explanation for the divergence in the bioactivity that existed among our newly synthesized derivatives against both COX-2 and sEH enzymes, a molecular docking study was conducted employing the freely available Autodock Vina program, version 1.1.2 [51, 52]. The 3D crystal structures of sEH (PDB code: 1VJ5) and COX-2 (PDB code: 5KIR) retrieved from Protein Data Bank (<https://www.rcsb.org>) were utilized for this purpose. This study would unveil some structural insights into their binding patterns and key interactions with COX-2 and sEH enzymes. Accordingly, the most active compounds **22** and **29** in addition to some other inactive or least active ones **30** and **31**, for comparison, were selected to be docked inside the active sites of both targets. Interestingly enough, the most/least active compounds were the same on both enzymes. Initially, a validation process of the docking methodology into COX-2 was performed through redocking the co-crystallized ligand, Rofecoxib into the binding site using the assigned protocol settings. The redocked results of this study revealed the superposition of the redocked rofecoxib over the co-crystallized ligands with RMDS of 1.32 Å using UCSF Chimera software version 1.15 [53] suggesting that the proposed protocol is acceptable and valid for the analysis of binding modalities of the tested compounds. Also, it was found that the redocked pose involved in similar interactions to that of co-crystallized ligand including H-bonding with Arg-513 residue and some other hydrophobic interactions, **Fig. 3 (A-C)**.

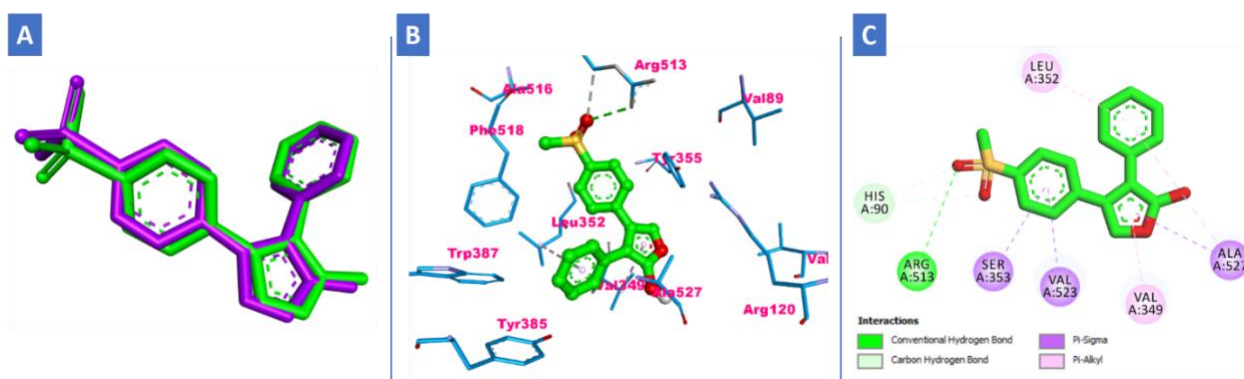


Fig. 3. A) Overlay of the redocked rofecoxib (shown as sticks, colored in green) and the co-crystallized ligand (shown as sticks, colored in violet) with RMSD of 1.34 Å; B) 3D Binding mode and interactions of redocked rofecoxib into COX-2 active site (PDB code: 5KIR); C) 2D binding mode of the redocked rofecoxib into COX-2 active site showing different types of interactions. H-bonds were represented as dashed green lines. All hydrogens were removed for the purposes of clarity.

The top two pyrazole-3-carboxamide derivatives with the most COX-2 inhibitory activity, **22** and **29**, as well as the two derivatives with the least inhibitory activity, **30** and **31**, were initially docked into the active pocket of COX-2. The results revealed that compounds **22** and **29** adopted a common binding mode similar to rofecoxib, with the diaryl pyrazole scaffold buried deep into the active site and the extended arm composed of 4-morpholin-4-yl phenethyl carboxamide located near the active site's entrance and exposed outward. In compounds **22** and **29**, one of the two nitrogen atoms of the pyrazole ring and the NH of the carboxamide moiety formed two important H-bonding interactions with the key-residue in the active site Tyr-355 amino acid. Moreover, in both **22** and **29**, the oxygen atom of the extended 4-morpholine moiety was involved in an additional H-bonding with the Tyr-115 residue.

Detailed analysis revealed that the pyrazole ring and the phenyl group of the phenethyl moiety in compound **22** was involved in two π -cation interactions with the residue Arg-120. In addition, one of the two phenyl groups attached to pyrazole formed π -sigma interaction with Val-523 residue. Finally, compounds **22** and **29** were involved in several hydrophilic interactions with Val-116, Val-349, Leu-352, Tyr-385, Trp-387, Phe-518 and Ala-527 amino acid residues. Due to the presence of an additional chlorine atom in **29**, the compound was forced to twist through the carboxamide linker to avoid some clashes, resulting in the loss of some pi interactions and a slight decrease in activity when compared to **22** ($IC_{50} = 0.82$ and 0.74 M, respectively). The 2D and 3D binding interactions of **22** and **29** within the active site of the COX-2 enzyme were shown in **Fig. 4(A-D)**.

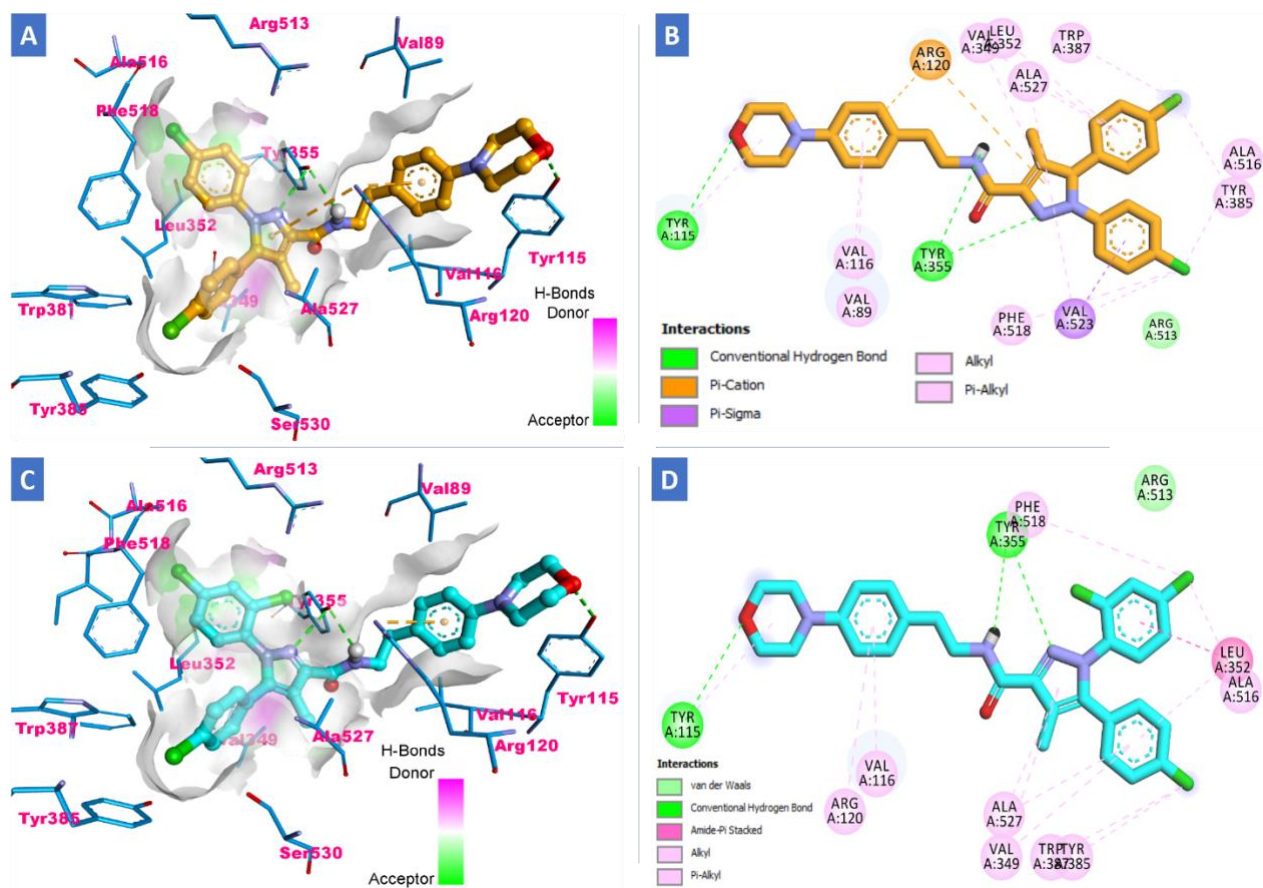


Fig. 4. Comparison of docking and 2/3D binding modes of compound **22** (Stick/Ball and stick with carbons colored in orange) and compound **29** (Stick/Ball and stick with carbons colored in cyan) within the catalytic active site of COX-2 enzyme (PDB code: 5KIR); **A**) 3D binding mode of compound **22** into active site of COX-2 enzyme; **B**) 2D Docking mode of **22** showing different types of interactions inside the active site of COX-2 enzyme; **C**) 3D binding mode of compound **29** into active site of COX-2 enzyme; **D**) 2D Docking mode of **29** showing different types of interactions inside the active site of COX-2 enzyme. H-bonds were represented as dashed green lines. All hydrogens were removed for the purposes of clarity. H-bond surfaces around ligands were created.

Meanwhile, compound **30** with the benzyl piperidine moiety was docked, and the results showed that fits nicely inside the active pocket without forming any H-bonds with the key residues, as shown in **Fig. 5(A-B)**. Furthermore, the difference in the length of the extension tethered to diaryl pyrazole between **30** and compounds **22** and **29** resulted in the loss of one important H-bonding with the Tyr-115 residue, which was easily approached by the morpholine ring. The superior bioactivity of **22** over **30** ($IC_{50} = 2.33$ M) could be attributed to the extra length and H-bonding, which were visible in **Fig. 5C** through the overlay of both **22** and **30**. The docking results of the least active compound **31** ($IC_{50} = 3.23$ M) revealed a completely inverse binding pattern and alignment without the formation of any critical H-bonding interactions. It was only involved in a few hydrophobic and π - π stacking interactions, as shown in **Fig. 5D**. Compound **31** protruded outside the pocket due to its inverse orientation, depriving it of important interactions.

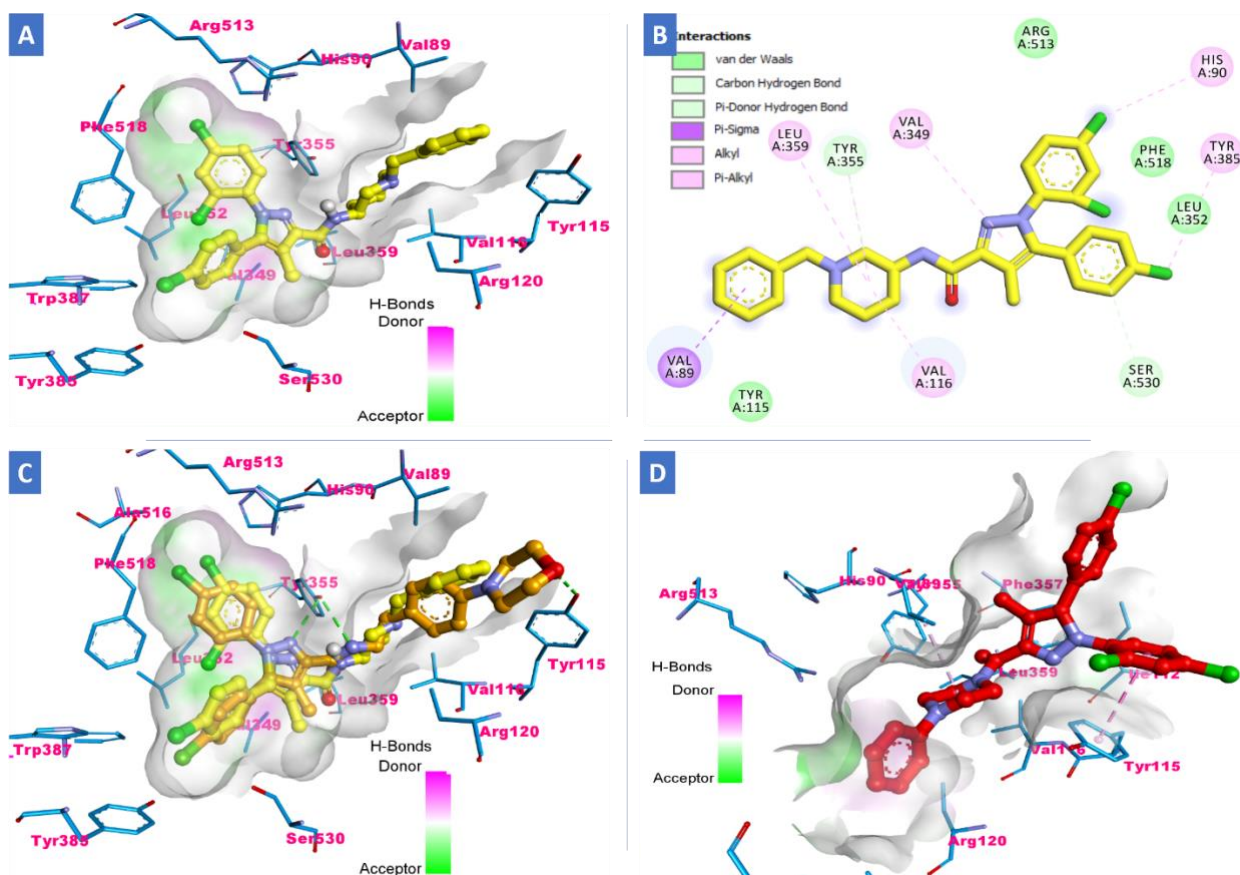


Fig. 5. Comparison of docking and 2/3D binding modes of compound **30** (Stick/Ball and stick with carbons colored in yellow) and compound **31** (Ball and stick with carbons colored in red) within the catalytic active site of COX-2 enzyme (PDB code: 5KIR); **A**) 3D binding mode of compound **30** into active site of COX-2 enzyme; **B**) 2D Docking mode of **30** showing different types of interactions inside the active site of COX-2 enzyme; **C**) Overlay of compound **22** and **30** into active site of COX-2 enzyme showing the difference in length and interactions; **D**) 3D binding mode of compound **31** into active site of COX-2 enzyme. H-bonds were represented as dashed green lines. All hydrogens were removed for the purposes of clarity. H-bond surfaces around ligands were created.

In addition to the investigation of binding modalities of the compounds and study of their interactions, the docking scores recorded by Autodock Vina (Binding affinity, ΔG (kcal/mol) for this simulation were consistent with the *in vitro* results and our explanation for the binding patterns. The binding affinities recorded by the docking software for the compounds **22**, **29**, **30** and **31** were -11.6, -10.6, -9.2 and -8.4 kcal/mol, respectively. Finally, the overlay of the top docking poses **22** and **29** with the co-crystallized ligand into COX-2 binding pocket showed good shape complementarity while compound **31** adopted an inverse positioning and alignment, **Fig. 6(A-C)**.

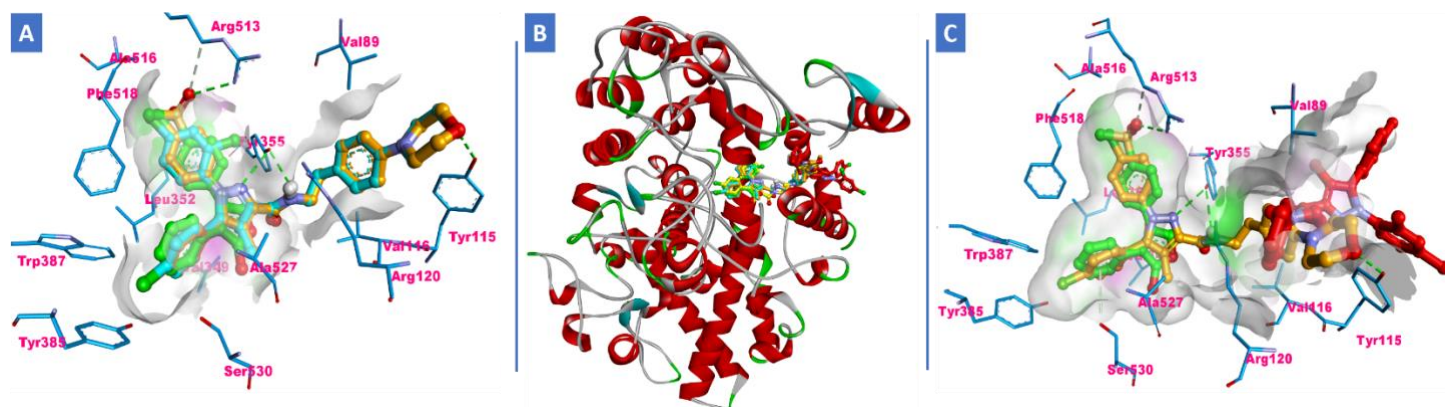


Fig. 6. **A)** Overlay of the top docked poses **22** (orange), **29** (cyan) and **rofecoxib** (green) as a co-crystallized ligand into the COX-2 binding pocket (PDB code: 5KIR); **B)** Superposition of **22**, **29**, **30**, **31** and **rofecoxib** into the active site of COX-2 protein represented as secondary structure displayed in a flat ribbon style; **C)** Overlay of the docked poses **22** (orange), **31** (red) and **rofecoxib** (green) into the COX-2 binding pocket to compare their different binding patterns.

On the other hand, the docking results of the two most active derivatives **22** and **29** into the active site of sEH showed that the top docked poses adopted a common binding pattern and modality where the diaryl pyrazole scaffold was located near the entrance of the active pocket and exposed outward while the 4-morpholin-4-yl phenethyl carboxamide extension was leaned in the catalytic pocket of sEH composed of the three main amino acids; Asp333, Tyr381, Tyr465 which are responsible for the activity of the enzyme, **Fig. 7(A-D)** [54, 55]. It was worth noting that this extended moiety in both **22** and **29** shared the same orientation and positioning of the co-crystallized ligand CIU in the catalytic pocket, **Fig. 7(D)**. Also, the amide moiety in compound **22** was engaged in two important H-bonding interactions with Gln-382 residue while phenyl morpholine moiety was involved in some π - π stacking with Tyr-381, His-523, and Tyr-524 amino acid residues, **Fig. 7(A-B)**. Moreover, the diaryl pyrazole bearing *p*-chloro substitutes in the two compounds **22** and **29** aligned towards Met-337, Trp-341, Ala-363, Trp-472, and Ala-475 residues forming hydrophobic interactions. It was found also that the pyrazole ring was involved in π -sulfur interactions with Met-468, Met-308 and Met-337, respectively. Finally, the diaryl core formed π - π stacking with Pro-369 and Trp-341 amino acids. It was conceptualized that the slight difference in inhibitory activities between **22** and **29** ($IC_{50} = 0.78$ and 0.84 nM, respectively) could be attributed to the absence of some H-bonding interactions and clashes that might be existed as a result of the extra chlorine atom in **29**.

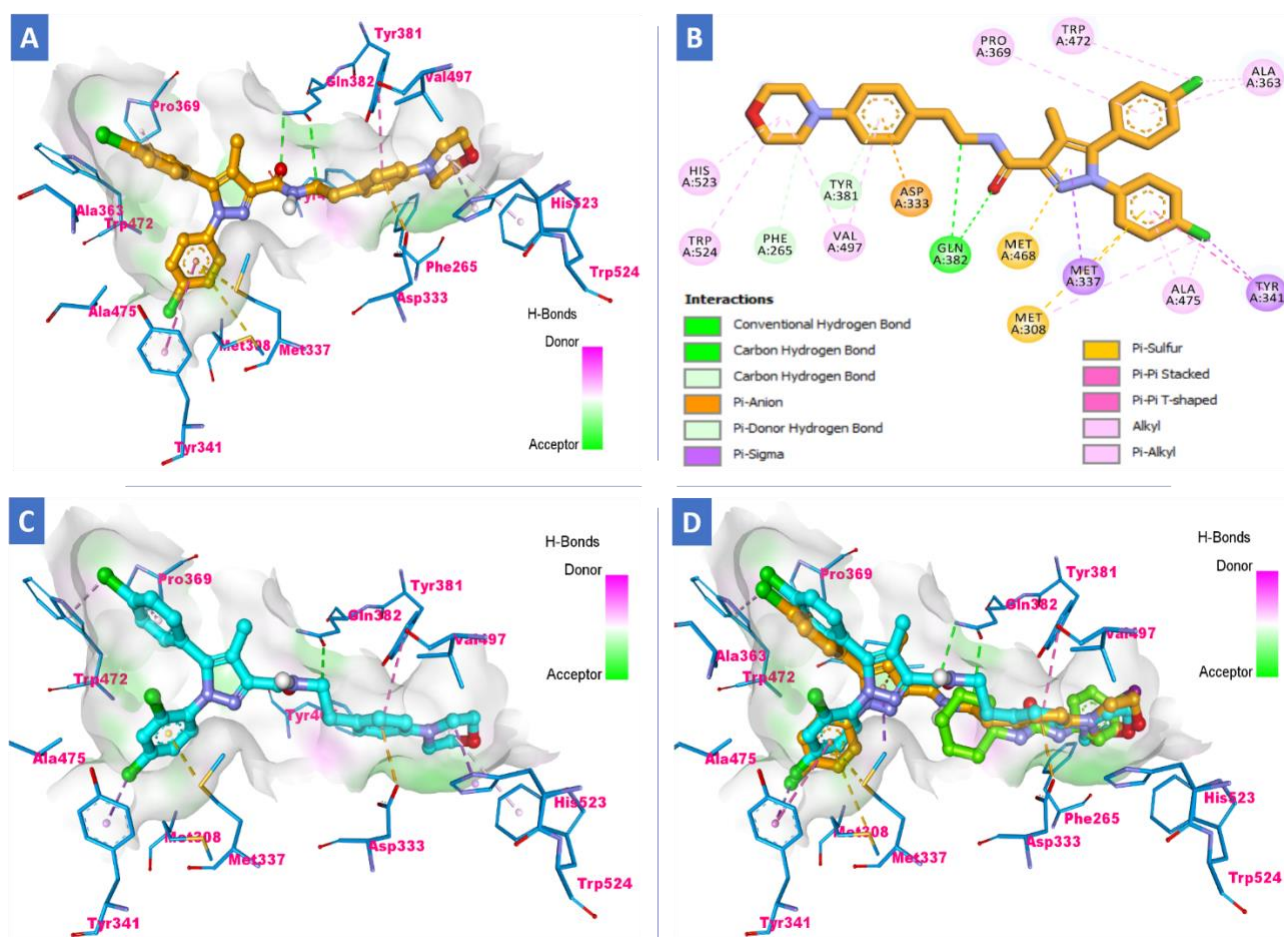


Fig. 7. Comparison of docking and 2/3D binding modes of compound **22** (Stick and stick/ball with carbons colored in orange) and compound **29** (Ball and stick with carbons colored in cyan) within the catalytic active site of sEH enzyme (PDB code: 1VJ5); **A**) 3D binding mode of compound **22** into active site of sEH enzyme; **B**) 2D Docking mode of **22** showing different types of interactions inside the active site of sEH enzyme; **C**) 3D binding mode of compound **29** into active site of sEH enzyme; **D**) Overlay of compound **22**, **29** and co-crystallized ligand, **CIU** (colored in green) into active site of sEH enzyme showing their alignment and interactions. H-bonds were represented as dashed green lines. All hydrogens were removed for the purposes of clarity. H-bond surfaces around ligands were created.

On the contrary, compounds **30** and **31** showed the least activity against the sEH enzyme with IC_{50} values of 4.1 and 4.7 nM, respectively. The examination of the docking results indicated that these two ligands shared a completely different alignment and orientation compared with the previously docked active derivatives **22** and **29**, **Fig. 8(A-D)**. It was found that the benzyl piperidine carboxamide and phenyl piperazin moieties in **30** and **31**, respectively protrude

outside the active pocket of sEH enzyme while, the diaryl pyrazole core buried deep into the extended part of the active site surrounded by Met-337, Try-341, Ilu-361, Pro-369, Gln-382, Met-368 and Trp-472 engaging only in some hydrophobic interactions without forming any H-bonds. Thus, the catalytic room (Asp333, Tyr381, and Tyr465) of the active site has become out of reach for these two ligands due to their different binding patterns and opposed dispositions. This great variation could be observed upon superposition of **30** and **31** with the co-crystallized ligand, **CIU** owing to the inferior activities compared to **CIU**, **Fig. 8(D)**. The docking scores recorded by Autodock Vina in terms of binding affinities, ΔG (kcal/mol) for this study were in line with the *in vitro* activities and our findings where compounds **22**, **29**, **30** and **31** revealed docking scores of -10.4, -10.3, -8.7 and -8.5 kcal/mol, respectively. Taken together, the docking simulation, along with the *in vitro* assay results, support the promising hybridization approach between the amide sEH pharmacophoric group and the diaryl pyrazole COX-2 core to develop potent leads for further optimization as anti-inflammatory agents with fewer cardiovascular risks.

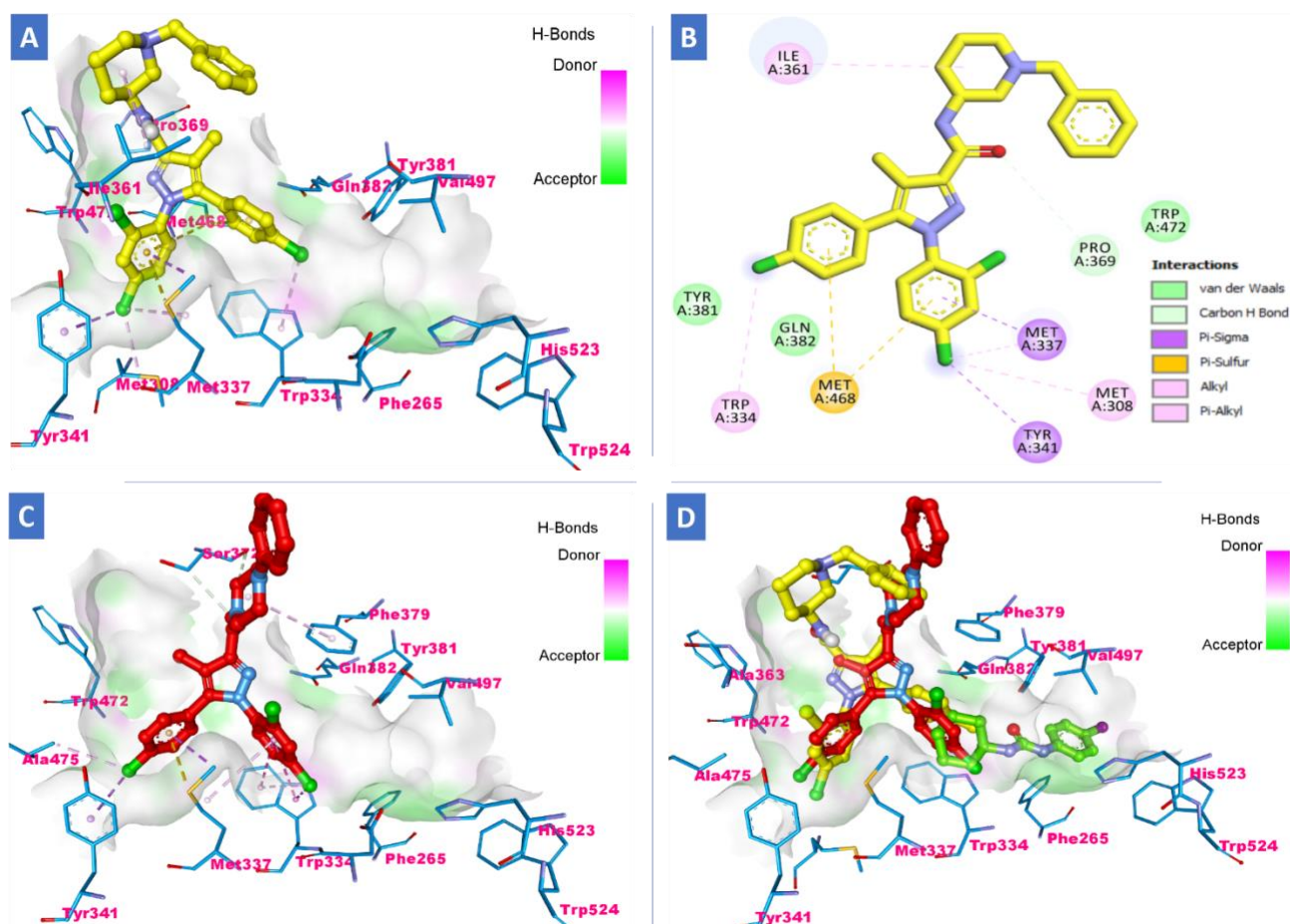


Fig. 8. Comparison of docking and 2/3D binding modes of compound **30** (Stick and stick/ball with carbons colored in yellow) and compound **31** (Ball and stick with carbons colored in red) within the catalytic active site of sEH enzyme (PDB code: 1VJ5); **A**) 3D binding mode of compound **30** into active site of sEH enzyme; **B**) 2D Docking mode of **30** showing different types of interactions inside the active site of sEH enzyme; **C**) 3D binding mode of compound **31** into active site of sEH enzyme; **D**) Overlay of compound **30**, **31** and co-crystallized ligand, **CIU** (colored in green) into active site of sEH enzyme showing their different alignments and interactions. H-bonds were represented as dashed green lines. All hydrogens were removed for the purposes of clarity. H-bond surfaces around ligands were created.

3. CONCLUSIONS

Novel series of 1,5-diaryl pyrazole-3-carboxamides **19-31** were synthesized and evaluated against COX-1, COX-2, and sEH enzymes as dual COX-2/sEH inhibitors. The most active dual inhibitors **20**, **22**, **29** showed, *in vivo*, potent analgesic, and anti-inflammatory biological outcomes, all of which are higher than celecoxib with lower ulcerogenicity. In terms of the cardiovascular system, the results confirmed that **22** and **29** are less cardiotoxic than the reference celecoxib. This was demonstrated by lower levels of diagnostic biomarkers of myocardial damage, such as LDH, Tn-I, TNF-, and CK-MB, as well as the inflammatory markers PGE2 and IL6.

4. Experimental

4.1. Chemistry

General Details: See Appendix A

Compounds **5-8** and **10** [32], **14-18** [33] were prepared as reported earlier.

General procedure for synthesis of indole-2-carboxamide derivatives 19-31

A mixture of the appropriate indole-2-carboxylic acids **17** and **18** (0.60 mmol, 1 eq.), BOP (1.5 eq.), and DIPEA (2 eq.) in DCM (30 mL) was stirred for 10 min at rt before adding the appropriate amine (1.2 eq.). The resulting reaction mixture was stirred overnight at rt. After vacuum removal of the solvent, the residue was extracted with EtOAc, washed with 5% HCl, saturated NaHCO₃ solution, brine, dried over MgSO₄, and evaporated under reduced pressure to yield a crude product that was purified by flash chromatography on silica gel to yield the final carboxamides **19-31**.

4.1.1. 1,5-bis(4-Chlorophenyl)-N-(4-(dimethylamino)phenethyl)-4-methyl-1H-pyrazole-3-carboxamide (19)

Yield % 80, mp 68-70 °C. ¹H NMR (400 MHz, δ ppm CDCl₃): δ 7.35 (d, *J* = 8.5 Hz, 2H, Ar-H), 7.26 (d, *J* = 8.8 Hz, 2H, Ar-H), 7.20 – 7.04 (m, 7H, Ar-H, amide NH), 6.71 (d, *J* = 8.6 Hz, 2H, Ar-H), 3.64 (q, *J* = 7.7 Hz, 2H, NHCH₂CH₂), 2.91 (s, 6H, N(CH₃)₂), 2.91 (t, *J* = 7.3 Hz, 2H, NHCH₂CH₂), 2.35 (s, 3H, CH₃). ¹³C NMR (101 MHz, CDCl₃) δ 162.70, 149.40, 144.59, 140.90, 137.91, 134.89, 133.41, 131.26, 129.45, 129.09, 127.91, 126.96, 125.90, 118.96, 113.03, 40.79, 40.69, 35.06, 9.37. HRESI-MS *m/z* calcd for [M+H]⁺ C₂₇H₂₇Cl₂N₄O: 493.1556, found: 493.1557.

4.1.2. 1,5-bis(4-Chlorophenyl)-4-methyl-N-(4-(2-methylpyrrolidin-1-yl)phenethyl)-1H-pyrazole-3-carboxamide (20)

Yield % 81, mp 78-80 °C. ¹H NMR (400 MHz, δ ppm CDCl₃): δ 7.35 (d, J = 8.4 Hz, 2H, Ar-H), 7.72 (d, J = 8.5 Hz, 2H, Ar-H), 7.19 – 7.05 (m, 7H, Ar-H, amide NH), 6.56 (d, J = 8.5 Hz, 2H, Ar-H), 3.86 - 3.82 (m, 1H, pyrrolidin-H), 3.63 (q, J = 7.0 Hz, 2H, NHCH₂CH₂), 3.44 - 3.47 (m, 1H, pyrrolidin-H), 3.14 (q, J = 8.4 Hz, 1H, pyrrolidin-H), 2.83 (t, J = 7.3 Hz, 2H, NHCH₂CH₂), 2.35 (s, 3H, CH₃), 2.16 – 1.91 (m, 3H, pyrrolidin-H), 1.72 - 1.65 (m, 1H, pyrrolidin-H), 1.17 (d, J = 6.2 Hz, 3H, CHCH₃). ¹³C NMR (101 MHz, CDCl₃) δ 162.70, 144.61, 140.89, 137.92, 134.88, 133.40, 131.25, 129.58, 129.45, 129.40, 129.12, 127.92, 126.35, 125.89, 118.95, 111.97, 53.44, 40.78, 35.10, 33.08, 30.91, 23.29, 19.38, 9.35. HRESI-MS m/z calcd for [M+H]⁺ C₃₀H₃₁Cl₂N₄O: 533.1869, found: 533.1871.

4.1.3. 1,5-bis(4-Chlorophenyl)-4-methyl-N-(4-(piperidin-1-yl)phenethyl)-1H-pyrazole-3-carboxamide (21)

Yield % 82, mp 65-67 °C. ¹H NMR (400 MHz, δ ppm CDCl₃): δ 7.35 (d, J = 8.4 Hz, 2H, Ar-H), 7.27 (d, J = 8.8 Hz, 2H, Ar-H), 7.17 – 7.04 (m, 7H, Ar-H, amide NH), 6.89 (d, J = 8.6 Hz, 2H, Ar-H), 3.64 (q, J = 7.6 Hz, 2H, NHCH₂CH₂), 3.15 – 3.07 (m, 4H, piperidin-H), 2.84 (t, J = 7.3 Hz, 2H, NHCH₂CH₂), 2.34 (s, 3H, CH₃), 1.76 – 1.65 (m, 4H, piperidin-H), 1.61 – 1.50 (m, 2H, piperidin-H). ¹³C NMR (101 MHz, CDCl₃) δ 162.70, 150.90, 144.55, 140.92, 137.89, 134.90, 133.44, 131.25, 129.60, 129.37, 129.11, 129.08, 127.89, 125.91, 116.82, 50.90, 40.51, 35.13, 25.89, 24.28, 9.35. HRESI-MS m/z calcd for [M+H]⁺ C₃₀H₃₁Cl₂N₄O: 533.1869, found: 533.1870.

4.1.4. 1,5-bis(4-Chlorophenyl)-4-methyl-N-(4-morpholinophenethyl)-1H-pyrazole-3-carboxamide (22)

Yield % 78, mp 80-82 °C. ¹H NMR (400 MHz, δ ppm CDCl₃): δ 7.35 (d, *J* = 8.4 Hz, 2H, Ar-H), 7.28 (d, *J* = 8.7 Hz, 2H, Ar-H), 7.21 – 7.04 (m, 7H, Ar-H, amide NH), 6.87 (d, *J* = 8.6 Hz, 2H, Ar-H), 3.89 – 3.82 (m, 4H, morph-H), 3.65 (q, *J* = 7.7 Hz, 2H, NHCH₂CH₂), 3.16 – 3.09 (m, 4H, morph-H), 2.86 (t, *J* = 7.3 Hz, 2H, NHCH₂CH₂), 2.35 (s, 3H). ¹³C NMR (101 MHz, CDCl₃) δ 162.70, 149.87, 144.52, 140.96, 137.89, 134.92, 133.50, 131.23, 130.52, 129.54, 129.12, 129.09, 127.85, 125.92, 118.96, 115.97, 66.93, 49.56, 40.51, 35.18, 9.35. HRESI-MS *m/z* calcd for [M+H]⁺ C₂₉H₂₉Cl₂N₄O₂: 535.1662, found: 535.1662.

4.1.5. 1,5-bis(4-Chlorophenyl)-4-methyl-1H-pyrazol-3-yl)(4-phenylpiperazin-1-yl) methanone (23)

Yield % 76, mp 80-82 °C. ¹H NMR (400 MHz, δ ppm CDCl₃): δ 7.37 (d, *J* = 8.4 Hz, 2H, Ar-H), 7.33 – 7.23 (m, 4H, Ar-H), 7.19 – 7.08 (m, 4H, Ar-H), 6.95 (d, *J* = 8.0 Hz, 2H, Ar-H), 6.90 (t, *J* = 7.4 Hz, 1H, Ar-H), 4.02 (dt, *J* = 18.4, 5.2 Hz, 4H, piperazin-H), 3.27 (dt, *J* = 21.6, 5.3 Hz, 4H, piperazin-H), 2.19 (s, 3H, CH₃). ¹³C NMR (101 MHz, CDCl₃) δ 163.32, 151.05, 146.03, 140.03, 137.96, 134.91, 133.30, 131.13, 129.23, 129.14, 129.12, 127.99, 125.84, 120.46, 118.25, 116.66, 50.22, 49.54, 47.17, 42.12, 9.08. HRESI-MS *m/z* calcd for [M+H]⁺ C₂₇H₂₅Cl₂N₄O: 491.1400, found: 491.1400.

4.1.6. 5-(4-Chlorophenyl)-1-(2,4-dichlorophenyl)-4-methyl-N-phenethyl-1H-pyrazole-3-carboxamide (24)

Yield % 80, mp 128-130 °C. ¹H NMR (400 MHz, δ ppm CDCl₃): δ 7.43 (d, *J* = 2.2 Hz, 1H, Ar-H), 7.34 – 7.19 (m, 9H, Ar-H), 7.10 – 7.02 (m, 3H, Ar-H, amide NH), 3.67 (q, *J* = 7.1, 2H, NHCH₂CH₂), 2.93 (t, *J* = 7.6 Hz, 2H, NHCH₂CH₂), 2.39 (s, 3H, CH₃). ¹³C NMR (101 MHz, CDCl₃) δ 162.66, 144.95, 142.96, 139.03, 135.91, 135.88, 134.88, 132.95, 130.80,

130.44, 130.32, 128.88, 128.80, 128.55, 127.83, 127.22, 126.39, 117.69, 40.42, 36.11, 9.42.

HRESI-MS m/z calcd for $[M+H]^+$ $C_{25}H_{21}Cl_3N_3O$: 484.0745, found: 484.0745.

4.1.7. 5-(4-Chlorophenyl)-1-(2,4-dichlorophenyl)-*N*-(4-(dimethylamino)phenethyl)-4-methyl-1*H*-pyrazole-3-carboxamide (25)

Yield % 82, mp 72-74 °C. 1H NMR (400 MHz, δ ppm $CDCl_3$): δ 7.42 (d, $J = 2.1$ Hz, 1H, Ar-H), 7.33 – 7.22 (m, 4H, Ar-H), 7.13 (d, $J = 8.6$ Hz, 2H, Ar-H), 7.09 – 7.02 (m, 3H, Ar-H, amide NH), 6.70 (d, $J = 8.6$ Hz, 2H, Ar-H), 3.62 (q, $J = 7.7$ Hz, 2H, $NHCH_2CH_2$), 2.91 (s, 6H, $N(CH_3)_2$), 2.83 (t, $J = 8.1$ Hz, 2H, $NHCH_2CH_2$), 2.39 (s, 3H, CH_3). ^{13}C NMR (101 MHz, $CDCl_3$) δ 162.63, 149.37, 145.07, 142.89, 135.95, 135.83, 134.83, 132.94, 130.81, 130.50, 130.28, 129.40, 128.86, 127.81, 127.29, 126.97, 117.65, 113.03, 40.81, 40.74, 35.05, 9.44. HRESI-MS m/z calcd for $[M+H]^+$ $C_{27}H_{26}Cl_3N_4O$: 527.1167, found: 527.1171.

4.1.8. 5-(4-Chlorophenyl)-1-(2,4-dichlorophenyl)-4-methyl-*N*-(4-(pyrrolidin-1-yl)phenethyl)-1*H*-pyrazole-3-carboxamide (26)

Yield % 81, mp 87-89 °C. 1H NMR (400 MHz, δ ppm $CDCl_3$): δ 7.42 (d, $J = 2.1$ Hz, 1H, Ar-H), 7.34 – 7.23 (m, 4H, Ar-H), 7.14 – 7.03 (m, 5H, Ar-H, amide NH), 6.52 (d, $J = 8.5$ Hz, 2H, Ar-H), 3.62 (q, $J = 8.0$ Hz, 2H, $NHCH_2CH_2$), 3.29 – 3.21 (m, 4H, pyrrolidin-H), 2.82 (t, $J = 8.1$ Hz, 2H, $NHCH_2CH_2$), 2.40 (s, 3H, CH_3), 2.02 – 1.94 (m, 4H, pyrrolidin-H). ^{13}C NMR (101 MHz, $CDCl_3$) δ 162.64, 146.68, 145.11, 142.89, 135.98, 135.81, 134.82, 132.94, 130.83, 130.54, 130.26, 129.47, 128.86, 127.82, 127.32, 125.51, 117.63, 111.85, 47.70, 40.89, 35.13, 25.45, 9.46. HRESI-MS m/z calcd for $[M+H]^+$ $C_{29}H_{28}Cl_3N_4O$: 553.1323, found: 553.1323.

4.1.9. 5-(4-Chlorophenyl)-1-(2,4-dichlorophenyl)-4-methyl-N-(4-(2-methylpyrrolidin-1-yl)phenethyl)-1H-pyrazole-3-carboxamide (27)

Yield % 78, mp 85-87 °C. ¹H NMR (400 MHz, δ ppm CDCl₃): δ 7.42 (d, J = 2.1 Hz, 1H, Ar-H), 7.33 – 7.22 (m, 4H, Ar-H), 7.13 – 7.02 (m, 5H, Ar-H, amide NH), 6.53 (d, J = 8.5 Hz, 2H, Ar-H), 3.88 – 3.79 (m, 1H, pyrrolidin-H), 3.62 (q, J = 7.2 Hz, 2H, NHCH₂CH₂), 3.40 (t, J = 8.6 Hz, 1H, pyrrolidin-H), 3.18 – 3.07 (m, 1H, pyrrolidin-H), 2.81 (t, J = 7.4 Hz, 2H, NHCH₂CH₂), 2.39 (s, 3H, CH₃), 2.14 – 1.90 (m, 3H, pyrrolidin-H), 1.73 – 1.64 (m, 1H, pyrrolidin-H), 1.16 (d, J = 6.2 Hz, 3H, CHCH₃). ¹³C NMR (101 MHz, CDCl₃) δ 162.64, 145.91, 145.10, 142.88, 135.96, 135.81, 134.82, 132.94, 130.80, 130.50, 130.27, 129.52, 128.85, 127.79, 127.30, 125.28, 117.64, 111.91, 53.68, 48.30, 40.85, 35.08, 33.11, 23.31, 19.44, 9.43. HRESI-MS m/z calcd for [M+H]⁺ C₃₀H₃₀Cl₃N₄O: 567.1480, found: 567.1484.

4.1.10. 5-(4-Chlorophenyl)-1-(2,4-dichlorophenyl)-4-methyl-N-(4-(piperidin-1-yl)phenethyl)-1H-pyrazole-3-carboxamide (28)

Yield % 78, mp 80-82 °C. ¹H NMR (400 MHz, δ ppm CDCl₃): δ 7.42 (d, J = 2.2 Hz, 1H, Ar-H), 7.31 – 7.23 (m, 4H, Ar-H), 7.12 (d, J = 8.6 Hz, 2H, Ar-H), 7.08 – 7.00 (m, 3H, Ar-H, amide NH), 6.88 (d, J = 8.6 Hz, 2H, Ar-H), 3.63 (q, J = 7.6 Hz, 2H, NHCH₂CH₂), 3.14 – 3.07 (m, 4H, piperidin-H), 2.83 (t, J = 7.6 Hz, 2H, NHCH₂CH₂), 2.38 (s, 3H, CH₃), 1.73 - 1.66 (m, 4H, piperidin-H), 1.61 – 1.51 (m, 2H, piperidin-H). ¹³C NMR (101 MHz, CDCl₃) δ 162.62, 150.85, 145.03, 142.90, 135.95, 135.83, 134.84, 132.95, 130.80, 130.50, 130.28, 129.58, 129.33, 128.86, 127.81, 127.27, 117.65, 116.79, 50.88, 40.56, 35.13, 25.89, 24.28, 9.42. HRESI-MS m/z calcd for [M+H]⁺ C₃₀H₃₀Cl₃N₄O: 567.1480, found: 567.1479.

4.1.11. 5-(4-Chlorophenyl)-1-(2,4-dichlorophenyl)-4-methyl-N-(4-morpholinophenethyl)-1H-pyrazole-3-carboxamide (29)

Yield % 79, mp 90-92 °C. ¹H NMR (400 MHz, δ ppm CDCl₃):) δ 7.42 (d, *J* = 2.2 Hz, 1H, Ar-H), 7.32 – 7.21 (m, 4H, Ar-H), 7.15 (d, *J* = 8.6 Hz, 2H, Ar-H), 7.09 – 7.01 (m, 3H, Ar-H, amide NH), 6.85 (d, *J* = 8.6 Hz, 2H, Ar-H), 3.87 – 3.80 (m, 4H, morph-H), 3.62 (q, *J* = 8.0 Hz, 2H, NHCH₂CH₂), 3.14 – 3.07 (m, 4H, morph-H), 2.84 (t, *J* = 8.1 Hz, 2H, NHCH₂CH₂), 2.38 (s, 3H). ¹³C NMR (101 MHz, CDCl₃) δ 162.63, 149.84, 144.99, 142.93, 135.92, 135.86, 134.86, 132.94, 130.80, 130.50, 130.48, 130.29, 129.51, 128.87, 127.83, 127.23, 117.66, 115.96, 66.92, 49.55, 40.56, 35.14, 9.43. HRESI-MS *m/z* calcd for [M+H]⁺ C₂₉H₂₈Cl₃N₄O₂: 569.1272, found: 569.1279.

4.1.12. N-(1-Benzylpiperidin-3-yl)-5-(4-chlorophenyl)-1-(2,4-dichlorophenyl)-4-methyl-1H-pyrazole-3-carboxamide (30)

Yield % 76, mp 80-82 °C. ¹H NMR (400 MHz, δ ppm CDCl₃):) δ 7.45 (d, *J* = 1.9 Hz, 1H, Ar-H), 7.35 – 7.18 (m, 9H, Ar-H), 7.07 (d, *J* = 8.5 Hz, 2H, Ar-H), 4.29 – 4.20 (m, 1H, piperidin-H), 3.52 (q, *J* = 12.4 Hz, 2H, PhCH₂), 2.65 - 2.60 (m, 1H, piperidin-H), 2.51 – 2.29 (m, 6H, piperidin-H, CH₃), 1.83 – 1.53 (m, 4H, piperidin-H). ¹³C NMR (101 MHz, CDCl₃) δ 161.82, 145.22, 142.83, 138.46, 136.11, 135.79, 134.79, 132.94, 130.80, 130.57, 130.29, 128.85, 128.15, 127.80, 127.39, 126.94, 117.61, 62.88, 58.22, 53.59, 45.01, 29.62, 22.54, 9.45. HRESI-MS *m/z* calcd for [M+H]⁺ C₂₉H₂₈Cl₃N₄O: 553.1323, found: 553.1323.

4.1.13. (5-(4-Chlorophenyl)-1-(2,4-dichlorophenyl)-4-methyl-1H-pyrazol-3-yl)(4-phenylpiperazin-1-yl)methanone (31)

Yield 75%, mp 83-85 °C. ¹H NMR (400 MHz, Chloroform-*d*) δ 7.44 (d, *J* = 2.2 Hz, 1H, Ar-H), 7.34 – 7.22 (m, 5H, Ar-H), 7.18 (d, *J* = 8.5 Hz, 1H, Ar-H), 7.08 (d, *J* = 8.5 Hz, 2H, Ar-H), 6.93 (d, *J* = 7.9 Hz, 2H, Ar-H), 6.88 (t, *J* = 7.3 Hz, 1H, Ar-H), 4.00 (dt, *J* = 19.6, 5.2 Hz,

4H, piperazin-H), 3.25 (dt, $J = 22.1, 5.1$ Hz, 4H, piperazin-H), 2.23 (s, 3H, CH_3). ^{13}C NMR (101 MHz, cdcl_3) δ 163.23, 151.05, 142.01, 135.94, 135.73, 134.84, 132.99, 130.69, 130.58, 130.30, 129.20, 128.94, 127.88, 127.33, 120.37, 117.09, 116.64, 50.15, 49.53, 47.21, 42.13, 9.14. HRESI-MS m/z calcd for $[\text{M}+\text{H}]^+$ $\text{C}_{27}\text{H}_{24}\text{Cl}_3\text{N}_4\text{O}$: 525.1010, found: 525.1016.

4.2. Pharmacological Evaluations

4.2.1. *In vitro* assays

4.2.1.1. COX-1 and COX-2 inhibition assays

All the newly synthesized 1,5-diaryl pyrazole-3-carboxamides **19-31** were screened for *in vitro* COX-1/COX-2 inhibition assays, using the COX-1/COX-2 (human) Inhibitor Screening Assay Kit [34]. **See Appendix A.**

4.2.1.2. Soluble epoxide hydrolase (sEH) assay

The inhibitory activity of the synthesized derivatives **19-31** against sEH enzyme using a cell-based assay kit [35] was evaluated *in vitro* and presented as IC₅₀ values. **See Appendix A.**

4.2.2. *In vivo* assays

4.2.2.1. Analgesic activity

Five compounds (**20-22**, **24**, and **29**) were selected to be examined for *in vivo* analgesic activity using the acetic acid-induced writhing method [36]. The reduction in acetic acid-induced writhing episodes was used to determine the efficacy and potency of the tested compounds. **See Appendix A.**

4.2.2.2. Anti-inflammatory assay

Five compounds (**20-22**, **24**, and **29**) were selected to be examined for *in vivo* anti-inflammatory activity using Winter et al. carrageen-induced paw edema bioassay method [37]. The compounds' efficacy was measured as the decrease in edema paw volume and calculated as edema inhibition percentage (EI %) after 1, 3, and 5 h of carrageenan injection versus the standard drug celecoxib. **See Appendix A**

4.3. Gastric ulcerogenic activity

The ulcerogenic effects of compounds **20**, **22**, and **29** were assessed by macroscopic observation of rat's intestinal mucosa following the oral use of 10 mg/kg of **20**, **22**, and **29** as well as indomethacin and celecoxib [38, 39]. **See Appendix A.**

4.4. Effect on inflammatory cytokines

Assessment of inflammatory cytokines PGE₂, IL-6 and TNF- α were determined using specific ELISA kits according to the manufacturer's instructions. All the parameters are measured using OD 450 nm [40-44]. **See Appendix A.**

4.5. Cardiovascular evaluation

Troponin-I (cTn-I) levels in serum were determined using ELISA kits and the reported method [56]. Levels of LDH and CK-MB were determined spectrophotometry [57, 58]. **See Appendix A.**

Acknowledgment

The authors extend their appreciation to the Deanship of Scientific Research at Jouf University for funding this work through research grant number (**DSR2020-04-421**)

References

- [1] H.H. Hassanein, H.H. Georgey, M.A. Fouad, A.M.E. Kerdawy, M.F. Said, Synthesis and molecular docking of new imidazoquinazolinones as analgesic agents and selective COX-2 inhibitors, *Future Med. Chem.* 9 (2017) 553-578.
- [2] E.M. Gedawy, A.E. Kassab, A.M.E. Kerdawy, Design, synthesis, and biological evaluation of novel pyrazole sulfonamide derivatives as dual COX-2/5-LOX inhibitors, *Eur. J. Med. Chem.* 189 (2020) 112066.
- [3] F.A. Ragab, N.M.A. Gawad, H.H. Georgey, M.F. Said, Synthesis of novel 1,3,4-trisubstituted pyrazoles as anti-inflammatory and analgesic agents, *Eur. J. Med. Chem.* 63 (2013) 645-654.
- [4] J.R.D. Vane, Frs, R.M.P. Botting, Mechanism of action of non-steroidal anti-inflammatory drugs, *Am. J. Med.* 104 (1998) 2S-8S.
- [5] H.U. Zeilhofer, Prostanoids in nociception and pain, *Biochem. Pharmacol.* 73 (2007) 165-174.
- [6] S.M. Stillman MJ, Choosing nonselective NSAIDs and selective COX-2 inhibitors in the elderly. A clinical use pathway. *Geriatrics* 62 (2007) 26-34.
- [7] D. Bishop-Bailey, J. A. Mitchell, T. D. Warner, COX-2 in Cardiovascular Disease, *Arterioscler. Thromb. Vasc. Biol.* 26 (2006) 956-958.
- [8] A.E. Enayetallah, R.A. French, M.S. Thibodeau, D.F. Grant, Distribution of soluble epoxide hydrolase and of cytochrome P450 2C8, 2C9, and 2J2 in human tissues, *J. Histochem. Cytochem.* 52 (2004) 447-454.
- [9] J.D. Imig, B.D. Hammock, Soluble epoxide hydrolase as a therapeutic target for cardiovascular diseases, *Nat. Rev. Drug Discov.* 8 (2009) 794-805.

- [10] A.A. Spector, X. Fang, G.D. Snyder, N.L. Weintraub, Epoxyeicosatrienoic acids (EETs): metabolism and biochemical function, *Prog. Lipid Res.* 43 (2004) 55-90.
- [11] K. Nithipatikom, G.J. Gross, Review article: epoxyeicosatrienoic acids: novel mediators of cardioprotection, *J. Cardiovasc Pharmacol. Ther.* 15 (2010) 112-119.
- [12] A. H. Abdelazeem, A. G. S. El-Din, M. M. Abdel-Fattah, N. H. Amin, S. M. El-Moghazy, M. T. El-Saadi. Discovery of novel urea-diaryl pyrazole hybrids as dual COX-2/sEH inhibitors with improved anti-inflammatory activity and highly reduced cardiovascular risks, *Eur. J. Med. Chem.* 205 (2020) 112662.
- [13] T. Yang, R. Peng, Y. Guo, L. Shen, S. Zhao, D. Xu, The role of 14,15-dihydroxyeicosatrienoic acid levels in inflammation and its relationship to lipoproteins, *Lipids Health Dis.* 12 (2013) 151.
- [14] K.M. Wagner, C.B. McReynolds, W.K. Schmidt, B.D. Hammock, Soluble epoxide hydrolase as a therapeutic target for pain, inflammatory and neurodegenerative diseases, *Pharmacol. Ther.* 180 (2017) 62-76.
- [15] G. Szabó, J. Fischer, A. Kis-Varga, K. Gyires, New Celecoxib Derivatives as Anti-Inflammatory Agents, *J. Med. Chem.* 21 (2008) 142-147.
- [16] A. P. Keche, G. D. Hatnapure, R. H. Tale, A. H. Rodge, V. M. Kamble. Synthesis, anti-inflammatory and antimicrobial evaluation of novel 1-acetyl-3,5-diaryl-4,5-dihydro (1H) pyrazole derivatives bearing urea, thiourea and sulfonamide moieties. *Bioorg. Med. Chem. Lett.* 22 (2012) 6611-6615.
- [17] N. Benaamane, B. Nedjar-Kolli, Y. Bentarzi, L. Hammal, A. Geronikaki, P. Eleftheriou, A. Lagunin. Synthesis and in silico biological activity evaluation of new N-substituted pyrazolo-oxazin-2-one systems. *Bioorg. Med. Chem.* 16 (2008) 3059-3066.

- [18] T. D. Penning, J. J. Talley, S. R. Bertenshaw, J. S. Carter, P. W. Collins, S. Docter, M. J. Graneto, L. F. Lee, J. W. Malecha, J. M. Miyashiro, R. S. Rogers, D. J. Rogier, S. S. Yu, G. D. Anderson, E. G. Burton, J. N. Cogburn, S. A. Gregory, C. M. Koboldt, W. E. Perkins, K. Seibert, A. W. Veenhuizen, Y. Y. Zhang, P. C. Isakson, Synthesis and Biological Evaluation of the 1,5-Diarylpyrazole Class of Cyclooxygenase-2 Inhibitors: Identification of 4-[5-(4-Methylphenyl)-3-(trifluoromethyl)-1*H*-pyrazol-1-yl]benzenesulfonamide (SC-58635, Celecoxib), *J. Med. Chem.* 40 (1997) 1347-1365.
- [19] G. Menozzi, L. Mosti, P. Fossa, F. Mattioli, M. Ghia. ω -Dialkylaminoalkyl ethers of phenyl-(5-substituted-1-phenyl-1*H*-pyrazol-4-yl)methanols with analgesic and anti-inflammatory activity. *J. Heterocycl. Chem.* 34 (1997) 963-968.
- [20] A. Balbi, M. Anzaldi, C. Macciò, C. Aiello, M. Mazzei, R. Gangemi, P. Castagnola, M. Miele, C. Rosano, M. Viale, Synthesis and biological evaluation of novel pyrazole derivatives with anticancer activity. *Eur. J. Med. Chem.* 46 (2011) 5293-5309.
- [21] I. Vujasinović, A. Paravić-Radičević, K. Mlinarić-Majerski, K. Brajša, B. Bertoša, Synthesis and biological validation of novel pyrazole derivatives with anticancer activity guided by 3D-QSAR analysis. *Bioorg. Med. Chem.* 20 (2012) 2101-2110.
- [22] H. Hashimoto, K. Imamura, J. I. Haruta, K. Wakitani, 4-(4-Cycloalkyl/aryl-oxazol-5-yl)benzenesulfonamides as Selective Cyclooxygenase-2 Inhibitors: Enhancement of the Selectivity by Introduction of a Fluorine Atom and Identification of a Potent, Highly Selective, and Orally Active COX-2 Inhibitor JTE-5221, *J. Med. Chem.* 45 (2002) 1511-1517.
- [23] A. G. Habeeb, P. N. Praveen Rao, E. E. Knaus, Design and Synthesis of Celecoxib and Rofecoxib Analogues as Selective Cyclooxygenase-2 (COX-2) Inhibitors: Replacement of

Sulfonamide and Methylsulfonyl Pharmacophores by an Azido Bioisostere. *J. Med. Chem.* 44 (2001) 3039-3042.

[24] M. H. Ismail, J. Lehmann, D. Abou El Ella, A. Albohy, K. M. Abouzid, Lonazolac analogues: molecular modelling, synthesis, and in vivo anti-inflammatory activity. *Med. Chem. Res.* 18 (2009) 725-744.

[25] N. K. Terrett, A. S. Bell, D. Brown, P. Ellis, Sildenafil (VIAGRATM), a potent and selective inhibitor of type 5 cGMP phosphodiesterase with utility for the treatment of male erectile dysfunction. *Bioorg. Med. Chem. Lett.* 6 (1996) 1819-1824.

[26] B. Costa, Rimonabant: More than an anti-obesity drug, *Br. J. Pharmacol.* 150 (2007) 535-537.

[27] J. H. M. Lange, C. G. Kruse, Keynote review: Medicinal chemistry strategies to CB1 cannabinoid receptor antagonists. *Drug Discov. Today* 10 (2005) 693-702.

[28] M. H. Abdelrahman, B. G. M. Youssif, M. A. abdelgawad, A. H. Abdelazeem, H. M. Ibrahim, A. A. Moustafa, L. Treamblu, S. N. A. Bukhari. Synthesis, Biological Evaluation, Docking Study and Ulcerogenicity Profiling of Some Novel Quinoline-2-Carboxamides as Dual COXs/LOX Inhibitors Endowed with Anti-Inflammatory Activity. *Eur. J. Med. Chem.* 127 (2017) 972-985.

[29] B. G. M. Youssif, M. F. A. Mohamed, M. M. Al-Sanea, A. H. Moustafa, A. A. Abdelhamid, H. A. M. Gomaa. Novel aryl carboximidamide and 3-aryl-1,2,4-oxadiazole analogues of naproxen as dual selective COX-2/15-LOX inhibitors: Design, synthesis and docking studies. *Bioorg. Chem.* 85 (2019) 577-584.

[30] S. A. Abdel-Aziz, E. S. Taher, P. Lan, G. F. Asaad, H. A. M. Gomaa, N. A. El-Koussi, B. G. M. Youssif, Design, synthesis, and biological evaluation of new pyrimidine-5-

carbonitrile derivatives bearing 1,3-thiazole moiety as novel anti-inflammatory EGFR inhibitors with cardiac safety profile. *Bioorg. Chem.* 111 (2021) 104890.

[31] K. R. A. Abdellatif, E. K.A. Abdelall, H. A.H. Elshemy, J. N. Philoppes, E. H. M. Hassanein, N. M. Kahk, Optimization of pyrazole-based compounds with 1,2,4-triazole-3-thiol moiety as selective COX-2 inhibitors cardioprotective drug candidates: Design, synthesis, cyclooxygenase inhibition, anti-inflammatory, ulcerogenicity, cardiovascular evaluation, and molecular modeling studies. *Bioorg. Chem.* 114 (2021) 105122.

[32] L. H. Al-Wahaibi, A. M. Gouda, O. F. Abou-Ghadir, O. I. A. Salem, A. T. Ali, H. S. Farghaly, M. H. Abdelrahman, L. Trembleau, H. H. M. Abdu-Allah, B. G. M. Youssif. Design and synthesis of novel 2,3-dihydropyrazino[1,2-a]indole-1,4-dione derivatives as antiproliferative EGFR and BRAF^{V600E} dual inhibitors. *Bioorg. Chem.* 104 (2020) 104260

[33] B.G. Youssif, A.M. Mohamed, E.E.A. Osman, O.F. Abou-Ghadir, D.H. Elnaggar, M.H. Abdelrahman, L. Treambu, H. A. Gomaa, 5-Chlorobenzofuran-2-carboxamides: From allosteric CB1 modulators to potential apoptotic antitumor agents, *Eur. J. Med. Chem.* 177 (2019) 1-11.

[34] E. M. Ahmed, A. E. Kassab, A. A. El-Malah, M. S. A. Hassan, Synthesis and biological evaluation of pyridazinone derivatives as selective COX-2 inhibitors and potential anti-inflammatory agents. *Eur. J. Med. Chem.* 171 (2019) 25-37.

[35] K.R. Schmelzer, B. Inceoglu, L. Kubala, I.H. Kim, S.L. Jinks, J.P. Eiserich, B.D. Hammock, Enhancement of anti-nociception by co-administration of nonsteroidal anti-inflammatory drugs and soluble epoxide hydrolase inhibitors, *Proc. Natl. Acad. Sci. U.S.A.* 103 (2006) 13646-13651

[36] D.B.E.J.R. Koster, M. Anderson, Acetic acid for analgesic screening, *Fed. Proc.* 18 (1959) 412.

- [37] C.A. Winter, E.A. Risley, G.W. Nuss, Carrageenin-induced edema in hind paw of the rat as an assay for anti-inflammatory drugs, *Proc. Soc. Exp. Biol. Med.* 111 (1962) 544-547.
- [38] E. Manivannan, S.C. Chaturvedi, Analogue-based design, synthesis and molecular docking analysis of 2, 3-diaryl quinazolinones as non-ulcerogenic anti-inflammatory agents, *Bioorg. Med. Chem.* 1 (2011) 4520-4528.
- [39] G. Clementi, A. Caruso, V.M.C. Cutuli, E. de Bernardis, A. Prato, N.G. Mangano, M. Amico-Roxas, Effects of centrally or peripherally injected adrenomedullin on reserpine-induced gastric lesions, *Eur. J. Pharmacol.* 360 (1998) 51-54.
- [40] G.S. Hassan, D.E. Abdel Rahman, E.A. Abdelmajeed, R.H. Refaey, M.A. Salem, Y. M. Nissan, New pyrazole derivatives: Synthesis, anti-inflammatory activity, cyclooxygenase inhibition assay and evaluation of mPGES, *Eur. J. Med. Chem.* 171 (2019) 332–342.
- [41] M.J. Fattahi, A. Mirshafiey, Prostaglandins and rheumatoid arthritis, *Arthritis* 2012 (2012) 239310.
- [42] C.S. Cardoso, D.P.B. Silva, D.M. Silva, et al., Mechanisms involved in the antinociceptive and anti-inflammatory effects of a new triazole derivative: 5-[1-(4-fluorophenyl)-1*H*-1,2,3-triazol-4-yl]-1*H*-tetrazole (LQFM-096), *Inflammopharmacology* 28 (2020) 877–892.
- [43] C.A. Hunter, S.A. Jones, IL-6 as a keystone cytokine in health and disease, *Nat. Immunol.* 16 (2015) 448-457.
- [44] S.B. Desai, D.E. Furst, Problems encountered during anti-tumor necrosis factor therapy, *Best. Pract. Res. Clin. Rheumatol.* 20 (2006) 757-790.
- [45] S. Ahmad, B. Prasad, K. Kohli, M. Fahim, K. Dubey, Folic acid ameliorates celecoxib cardiotoxicity in a doxorubicin heart failure rat model, *Pharmaceut. Biol.* 55 (2017) 1295-1303

- [46] S. Ahmad, B. Prasad, M. Fahim, N. Dhyani, K. Dubey, Ameliorative effect of beraprost sodium on celecoxib induced cardiotoxicity in rats, *Iran. J. Pharm. Res. (IJPR)* 17 (2018) 155-163.
- [47] A.G. Olatidoye, A.H.B. Wu, Y.-J. Feng, D. Waters, Prognostic role of troponin T versus troponin I in unstable Angina pectoris for cardiac events with metaanalysis comparing published studies, *Am. J. Cardiol.* 9149 (1998) 1405-1410.
- [48] K.H.S. Farvin, R. Anandan, S.H. Senthil, K.S. Shiny, T. V Sankar, T.K. Thankappan, Effect of squalene on tissue defense system in isoproterenol induced myocardial infarction in rats, *Pharmacol. Res.* 50 (2004) 231-236.
- [49] T. Tsutamoto, C. Kawahara, K. Nishiyama, M. Yamaji, Prognostic role of highly sensitive cardiac troponin I in patients with systolic heart failure, *Am. Heart J.* 159 (2010) 63-67.
- [50] Q. Zhou, X. Pan, L. Wang, X. Wang, D. Xiong, The protective role of neuregulin-1 : a potential therapy for sepsis-induced cardiomyopathy, *Eur. J. Pharmacol.* 788 (2016) 234-240.
- [51] O. Trott, A. J. Olson, AutoDock Vina: Improving the speed and accuracy of docking with a new scoring function, efficient optimization, and multithreading. *J. Comput. Chem.* 31 (2010) 455-461.
- [52] G.M. Morris, R. Huey, W. Lindstrom, M.F. Sanner, R.K. Belew, D.S. Goodsell, A. J. Olson, AutoDock4 and AutoDockTools4: Automated docking with selective receptor flexibility, *J. Comput. Chem.* 30 (2009) 2785–2791.
- [53] E.F. Pettersen, T.D. Goddard, C.C. Huang, G.S. Couch, D.M. Greenblatt, E.C. Meng, T.E. Ferrin, UCSF Chimera-a visualization system for exploratory research and analysis, *J. Comput. Chem.* 25 (2004) 1605-1612.

- [54] F.A.M. Mohamed, H. A.M. Gomaa, O.M. Hendawy, A.T. Ali , H. S. Farghaly, A. M. Gouda, A. H. Abdelazeem, M. H. Abdelrahman, L. Trembleau, B. G. M. Youssif. Design, synthesis, and biological evaluation of novel EGFR inhibitors containing 5-chloro-3-hydroxymethyl-indole-2-carboxamide scaffold with apoptotic antiproliferative activity. *Bioorg. Chem.* 112 (2021) 104960
- [55] BioVia, Discovery Studio Visualizer version 16.1.0.15350, San Diego, CA, USA (2017).
- [56] H.A. Katus, A. Remppis, S. Looser, K. Hallemeier, T. Scheffold, W. Kiibler, Enzyme linked immune of acute assay of cardiac troponin T for the myocardial infarction in patients, *J. Mol. Cell. Cardiol.* 353 (1989) 1349-1353.
- [57] P.S. Rao, J.J. Lukes, S.M.H. Ayres and Mueller, New manual and automated method for determining activity of creatine kinase isoenzyme MB, by use of dithiothreitol: clinical applications, *Clin. Chem.* 21 (1975) 1612-1618.
- [58] R.G. Martinek, A rapid ultraviolet spectrophotometric lactic dehydrogenase assay, *Clin. Chim. Acta* 40 (1972) 91-99.